



ORIGINAL ARTICLE

Het(aryl)isatin to het(aryl)aminoindoline scaffold hopping: A route to selective inhibitors of matrix metalloproteinases



Vladimir N. Ivanov^{a,1}, Mariangela Agamennone^{b,1}, Ildar R. Iusupov^a, Antonio Laghezza^c, Anton M. Novoselov^a, Ekaterina V. Manasova^{a,d}, Andrea Altieri^{a,d}, Paolo Tortorella^c, Alexander A. Shtil^{a,e}, Alexander V. Kurkin^{a,*}

^a Chemistry Department, Lomonosov Moscow State University, GSP-2, 1/3 Leninskie Gory, 119991 Moscow1, Russia

^b Department of Pharmacy, University "G. d'Annunzio" of Chieti-Pescara, Via dei Vestini 31, 66013 Chieti, Italy

^c Department of Pharmacy and Pharmaceutical Sciences, University of Bari "A. Moro", Via Orabona 4, 70126 Bari, Italy

^d EDASA Scientific srls, Via Stingi 37, 66050 San Salvo, Italy

^e Blokhin Cancer Center, 24 Kashirskoye shosse, 115478 Moscow, Russia

Received 10 July 2021; accepted 7 October 2021

Available online 18 October 2021

KEYWORDS

Matrix metalloproteinases;
MMP inhibitors;
Structure-based drug design;
Non-zinc binding;
Isatin;
Drug discovery

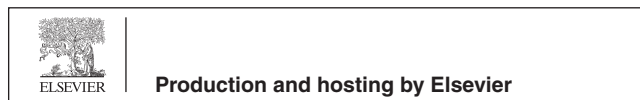
Abstract Matrix metalloproteinases (MMPs) are a large family of zinc-dependent endoproteases known to exert multiple regulatory roles in tumor progression. A variety of chemical classes have been explored for targeting individual MMP isoforms. In the present study, we further developed our isatin based scaffold **BB0223107** capable of binding to and inactivating MMP-2 in a zinc-independent manner (Agamennone et al., 2016). Forty four new compounds were synthesized based on the modified **BB0223107**. All compounds were tested in enzyme inhibition assays against MMP-2, -8 and -13. SAR studies demonstrated that 5-het(aryl)-3-aminoindolin-2-ones (**37–39**) were active toward MMP-2 and MMP-13. The most potent compounds **33** and **37** displayed an IC_{50} of 3 μ M against MMP-13 and showed a negligible activity toward MMP-8; almost all new compounds were inactive toward MMP-8. Replacement of the isatin ring with a biaryl system (compound **33**) did not decrease the potency against MMP-13 but reduced the selectivity. Structure-based computational studies were carried out to rationalize the inhibitory activity data. The analysis of binding geometries confirmed that all fragments occupied the S1' site in the three enzymes while no ligand was able to bind the catalytic zinc ion. To the best of our knowledge, this is the first example of 3-aminoindolin-2-one-based MMP inhibitors that, based on the computer

* Corresponding author.

E-mail address: kurkin@direction.chem.msu.ru (A.V. Kurkin).

¹ Equal contribution.

Peer review under responsibility of King Saud University.



modeling study, do not coordinate the zinc ion. Thus, the het(aryl)-3-aminoindolin-2-one derivatives emerge as a drug-like and promising chemotype that, along with the hetaryl variations, represents an alternative and thrifty tool for chemical space exploration aimed at MMP inhibitor design.

© 2021 The Authors. Published by Elsevier B.V. on behalf of King Saud University. This is an open access article under the CC BY-NC-ND license (<http://creativecommons.org/licenses/by-nc-nd/4.0/>).

1. Introduction

Matrix metalloproteinases (MMPs) are a family of zinc-dependent endoproteases with multiple roles in tissue remodeling and degradation of various proteins in the extracellular matrix (ECM) (Cui et al., 2017). MMPs divide into five clusters according to their function and structure (A, collagenases; B, gelatinases; C, stromelysins; D, membrane-type; E, matrilysins) (Amin et al., 2017). More than 25 MMPs have been currently identified and characterized (Adhikari et al., 2017). MMPs share common characteristics: they are initially biosynthesized as inactive zymogens (King, 2016), the cytosolic and the transmembrane portions are followed by the hemopexin-like domain, the hinge region, and a highly conserved catalytic domain that contains 160–170 amino acids with symmetrical pockets (Sn,...S2, S1; S1', S2', ...Sn'). Between these pockets, a sequence HEXHXXGXXH containing His218, His222, and His228 residues, along with water molecules, coordinates the catalytic zinc ion in the active site whereas another zinc ion is located in the S-loop (Fig. 1).

Zn²⁺ is coordinated by three histidine residues in the catalytic domain and a cysteine residue from the shared pro-domain. In this state, with the pro-domain occupying the active site, the enzyme is inactive. All MMPs are activated upon cleavage of the pro-domain and exposure of the active site (Fig. 1) (King, 2016).

MMPs have been involved in the cleavage of cell surface receptors, as well as in the release of the apoptotic Fas ligand (Sternlicht and Werb, 2001) and chemokine/cytokine inactivation (Young et al., 2019). Furthermore, MMPs play a role in cell proliferation, migration, adhesion, differentiation, angiogenesis, survival and host defense (Conlon and Murray, 2019; Winer et al., 2018; Cathcart et al., 2015; Zhong et al., 2018).

We focused on MMP-2, -13, and -8 because of their key, although differential, role in cancer progression. MMP-2 allows cell migration out of the primary site, a step to metastasis formation (Overall and Kleinfeld, 2006; Dufour and Overall, 2013). Specifically, MMP-2 is capable of degrading type IV collagen, the most abundant component of the basal membrane (Tauro and Lynch, 2018; Winer et al., 2016; Shay et al., 2017). Moreover, MMP-2 can be overexpressed along with histone deacetylase in blood malignancies (Amin et al., 2017). The hemopexin domain of MMP-13 participates in collagen degradation whereas the catalytic domain lacks this activity (Kudo et al., 2012). MMP-8 is a collagen cleavage enzyme. Also, MMP-8 degrades cytokines such as IL-8, thereby regulating the chemotaxis of neutrophils. This property is important for antitumor host defense (Juurikka et al., 2019; Thirkettle et al., 2013). Thus, the 'ideal' modulator should preferentially inhibit MMP-2 and MMP-13 but, at the same time, spare MMP-8 (Overall and Kleinfeld, 2006).

Initial clinical trials (Fields, 2019) and selectivity issues have been an obstacle for FDA approval of MMP inhibitors (Dufour and Overall, 2013; Vandembroucke and Libert, 2014). In fact, early MMP modulators were largely based on strong zinc-chelating agents such the hydroxamates (Fig. 2).

The hydroxamate-based inhibitors lack selectivity due to the binding of other metalloproteases and causing off-target effects (Vandembroucke and Libert, 2014). Moreover, the hydroxamic group is metabolically unstable (Fields, 2019). As an alternative to the hydroxamate (Fischer et al., 2019), milder Zn²⁺ chelators less prone to hydrolysis (i.e., Rebimastat, Fig. 2) have been explored, such as thiol, carboxylate, phosphonate, etc. Furthermore, interesting is the possibility to inhibit these enzymes by establishing an interaction with the S1' binding site in MMPs, called the primary specificity site (Fabre et al., 2014; Gimeno et al., 2020). This pocket is located next to the Zn²⁺ binding site. Unlike S1, S2, and S3 domains, the pocket presents diversity and therefore can be used in the design of selective, non-Zn²⁺-binding modulators of MMP-13 (Engel et al., 2005; Di Pizio et al., 2016), MMP-8 (Pochetti et al., 2009), MMP-12 (Dublanche et al., 2005) and MMP-2 (Di Pizio et al., 2013; Laghezza et al., 2020).

Previously we have reported the screening, analog selection and synthesis that yielded a promising fragment hit **BB0223107** (Fig. 3) with a micromolar potency (Agamennone et al., 2016).

As a starting point, in the present study, we used the isatin-based fragment **BB0223107** which showed selectivity to MMP-2 and MMP-13 (IC₅₀ ~ 6 μM) compared to MMP-8 (IC₅₀ = 57 μM), as well as promising ligand efficacy (LE = 0.5) (Agamennone et al., 2016). This result, in combination with the cost-effective synthesis, deserved further investigation. We intended to keep the core of **BB0223107** for the next series of inhibitors to explore SAR around this chemotype, that is, substitutions of the phenyl ring (cluster **A**), the isatin portion (cluster **B**), and modification of the carbonyl group at C3 (cluster **C**) (Fig. 3). Our results provided evidence that the switch from the isatin scaffold can be beneficial for the design of inhibitors with a preferential potency against MMP-2 and -13 whereas MMP-8 remains untouched.

2. Results and discussion

Based on the **BB0223107** synthetic pathway, isatin isosteric replacements, chemical feasibility and a drug-like guided peripheral decoration, a virtual tangible library of 1000 analogues was generated. The library was subjected to MMP-2 S1' pocked docking (Di Pizio et al., 2013) to identify the most promising compounds for synthesis. A total of 44 compounds out of this set was selected for synthesis. These compounds belong to three clusters (Fig. 4).

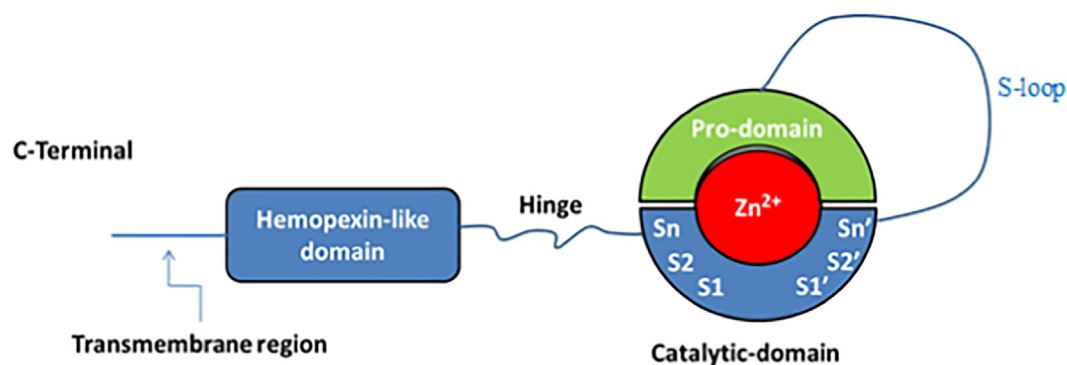


Fig. 1 Schematic representation of MMP structure.

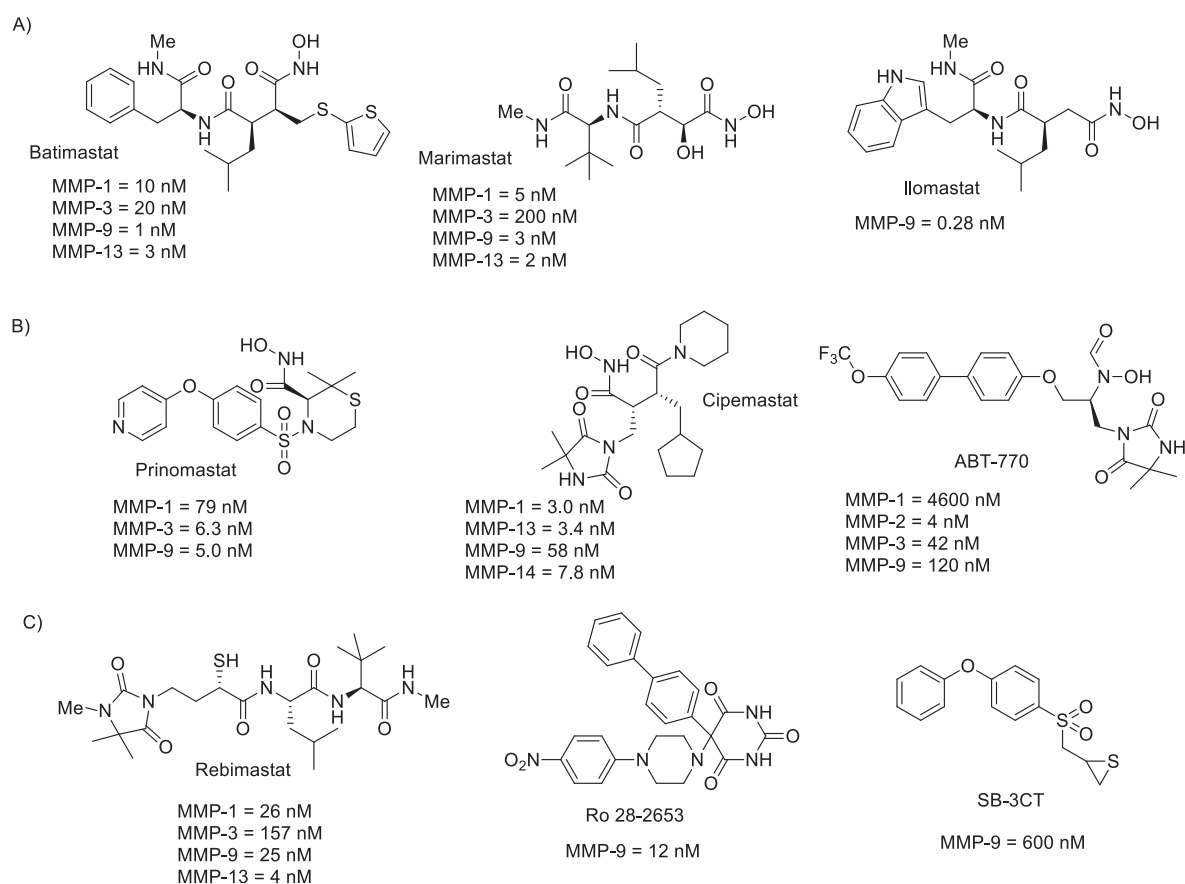


Fig. 2 MMP inhibitors: (A) Example of non-selective MMP hydroxamate-based inhibitors capable of strongly coordinating the interaction with Zn^{2+} cofactor. (B) Example of selective MMP hydroxamate-based inhibitors capable of strong coordination/interaction with Zn^{2+} cofactor. (C) Example of non-hydroxamate-based MMP selective inhibitors making ‘mild/soft’ Zn^{2+} coordination interactions.

2.1. Synthesis and testing of Cluster A compounds

We have previously reported the synthesis of 5-arylisatins from 5-bromoisatin and the boronic aryl derivatives by Suzuki cross-coupling reactions (Agamennone et al., 2016). Compounds **7**, **8**, **12**, **14**, **15**, **18**, **20–22**, **29–31** have been synthesized using the procedures applied for the synthesis of 5-arylisatins (Agamennone et al., 2016; Lisowski et al., 2000). Compound **19** was obtained by direct oxidation of **18**. Oxidation of **18** with

H_2O_2 in acetic acid at 100 °C led to the racemate **19** with a low yield (overall 6% from the starting 5-bromoisatin). The reaction proceeded with *ortho*- and *meta*-substituted boronic acid (**8**, **14**, **29–31**) and can tolerate diverse functional groups (**12** and **22**). Although the yields were low to moderate (5% for **22** and 76% for **7**), the simplicity of this method allowed us to prepare gram-scale quantities of 5-arylisatins **7**, **18**, **29–31**.

The synthesis of 5-arylisatin via arylboronic derivatives often generated side products difficult to purify and isolate.

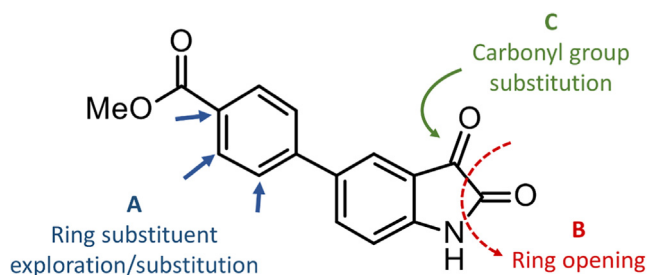


Fig. 3 Sites of chemical modifications of BB0223107.

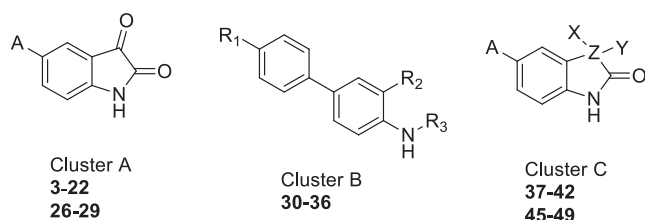
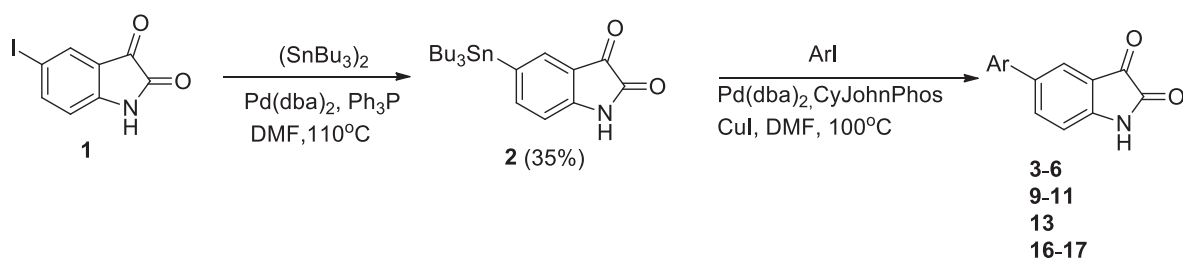
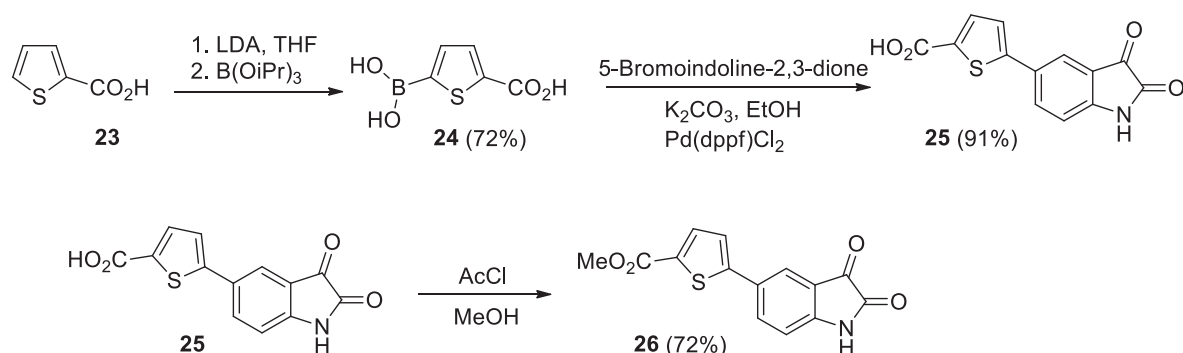


Fig. 4 Clustering of compounds selected for synthesis, Cluster A (24 isatin analogues) was used to explore SAR of the distal phenyl ring, Cluster B explores the activity variations in the case of isatin ring opening. Cluster C: modification of the carbonyl group at C3. A, Y, Z, X, Y, R1, R2 and R3 are indicated in Tables 1–3.

To overcome this issue, an alternative approach was implemented for the synthesis of **3–6**, **9–11**, **13**, **16** and **17** (Scheme 1). 5-(Tributylstannyl)isatin (**2**) was coupled with ten different iodoaryl derivatives by Stille coupling reaction to afford compounds **3–6**, **9–11**, **13**, **16** and **17** isolated in 12–59% yield (Scheme 1).



Scheme 1 The synthetic route for compounds **3–6**, **9–11**, **13**, **16**, **17**. Ar groups are indicated in Table 1.



Scheme 2 Synthesis of compound **26**.

Based on the fact that 5-(2-thienyl)-isatin **BB 0223104** (Agamennone et al., 2016; Zhang et al., 2018) showed a low micromolar potency toward MMP-13 ($IC_{50} = 2.7 \mu M$), we tested the isatin **26** in which phenyl ring is replaced with potential bioisosteric moieties. We hypothesized that methyl 5-(2,3-dioxindolin-5-yl)thiophene-2-carboxylate (**26**) can be interesting. Its synthesis required the corresponding acid since none of the strategies using aryl/heteroarylboronic acid or stannates were applicable. The synthesis of **26** is shown in Scheme 2.

All synthesized compounds were tested in the enzyme inhibition assays using the catalytic domain of MMP-2, MMP-8, and MMP-13 (Laghezza et al., 2020). Screening results for isatin-based compounds (Cluster A) are presented in Table 1. The data obtained from 1H NMR, ^{13}C NMR and mass spectrometry confirmed the proposed structures. Spectra are provided in the Supplementary material.

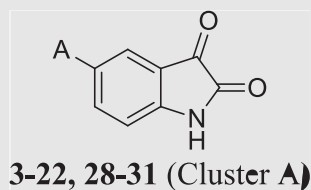
Table 1 shows that all compounds were inactive towards MMP-8 with the exception of **BB 0223107** ($IC_{50} = 57 \mu M$) and **26** ($IC_{50} = 14.5 \mu M$).

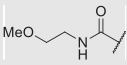
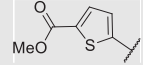
Table 1 shows that all compounds were inactive towards MMP-8 with the exception of **BB 0,223,107** ($IC_{50} = 57 \mu M$) and **26** ($IC_{50} = 14.5 \mu M$).

The most potent substituents in the phenyl ring at 5-position of the isatin core for MMP-2 and MMP-13 inhibition were at *para*-position (R_1) while *meta*-position (R_2) somewhat decreased the activity. The *ortho*-substitution, in particular, provides selective compounds toward MMP-2 (**10**, **13**: IC_{50} 55 μM and 21 μM , respectively) and MMP-13 (**14**: $IC_{50} = 3.7 \mu M$). As for R_1 the MMP-2 and MMP-13 activity changed in the row:

MMP-2:

$-COOMe$ ($IC_{50} = 6 \mu M$) > F- (**7**, $IC_{50} = 10 \mu M$) > $-SMe$ (**18**, $IC_{50} = 14 \mu M$), $-S(O)Me$ (**19**, $IC_{50} = 15 \mu M$) > NO_2 (**9**, $IC_{50} = 27 \mu M$) > CN (**12**, $IC_{50} = 29 \mu M$).

Table 1 MMP-2, MMP-8 and MMP-13 inhibition by isatin-based (Cluster A) compounds 3–22 and 26–29.

Compound ID	A				IC ₅₀ (μM) ^a		
	R ₁	R ₂	R ₃	Heteroaryl	MMP-2	MMP-8	MMP-13
BB 0223107 ^b	–COOMe	–H	–H	–	6.1 ± 0.7	57 ± 9	6.2 ± 0.6
3,	–H	–H	–COOMe	–	> 100	> 100	> 100
BB 0305124							
4,	–COOMe	–H	–Cl	–	18.7 ± 0.5	> 100	> 100
BB 0305116							
5,	–NHAc	–H	–H	–	> 100	> 100	> 100
BB 0304038							
6,	–F	–H	–Cl	–	> 100	> 100	> 100
BB 0305115							
7,	–F	–H	–H	–	10.2 ± 2.4	> 100	15.8 ± 1.6
BB 0223093							
8,	–H	–H	–F	–	> 100	> 100	> 100
BB 0223954							
9,	–NO ₂	–H	–H	–	26.9 ± 1.0	> 100	> 100
BB 0305121							
10,	–H	–H	–NO ₂	–	55.3 ± 3.7	> 100	> 100
BB 0305122							
11,	–H	–H	–Br	–	> 100	> 100	> 100
BB 0305120							
12,	–CN	–H	–H	–	29.1 ± 1.1	> 100	20.0 ± 2.0
BB 0223114							
13,	–H	–H	–CN	–	21.1 ± 1.6	> 100	> 100
BB 0305123							
14,	–H	–H	–OMe	–	> 100	> 100	37 ± 13
BB 0223102							
15,	–CF ₃	–H	–H	–	> 100	> 100	> 100
BB 0223115							
16,	–F	–Cl	–H	–	> 100	> 100	> 100
BB 0305130							
17,	–CH ₂ NHAc	–H	–H	–	> 100	> 100	> 100
BB 0305118							
18,	–SMe	–H	–H	–	14 ± 3	> 100	3.8 ± 2.1
BB 0223099							
19,	–S(O)Me	–H	–H	–	15 ± 5	> 100	6 ± 3
BB 0300735							
20,	–S(O) ₂ Me	–H	–H	–	> 100	> 100	> 100
BB 0223960							
21,	t–Bu–	–H	–H	–	> 100	> 100	87 ± 9
BB 0223799							
22,		–H	–H	–	33 ± 3	> 100	48 ± 7
BB 0300746							
26,							
BB 0300739					12 ± 6	14.5 ± 2.5	3.1 ± 0.5
27,	–H	–F	–H	–	> 100	> 100	57.1 ± 1.0
BB 0223094							

(continued on next page)

Table 1 (continued)

Compound ID	A				IC ₅₀ (μM) ^a		
	R ₁	R ₂	R ₃	Heteroaryl	MMP-2	MMP-8	MMP-13
28, BB 0223101	—H	—OMe	—H	—	> 100	> 100	> 100
29, BB 0223116	—H	—CF ₃	—H	—	> 100	> 100	18.6 ± 1.5
NNGH ^c					0.0972 ± 0.0124	0.0327 ± 0.0019	0.0307 ± 0.0057

^a Data represent mean ± SEM of at least three independent experiments in triplicate.

^b Published data (Agamennone et al., 2016).

^c Reference inhibitor: N-Isobutyl-N-(4-methoxyphenylsulfonyl)glycyl hydroxamic acid.

MMP-13:

—SMe (**18**, IC₅₀ = 4 μM) > —S(O)Me (**19**, IC₅₀ = 6 μM) > —COOMe (IC₅₀ = 6.2 μM) > F- (**7**, IC₅₀ = 16 μM) > CN (**12**, IC₅₀ = 20 μM).

These data confirmed our initial idea that the functional group in the *para*-position of the phenyl ring of the isatin core can form polar interactions in the binding site. For example, compounds **7**, **18**, and **19** as hydrogen bond acceptors for the OH group of Thr247 showed an increased activity. Regarding the activity of fluorine and thiol groups: electronic properties of the C — F bond allowed to mimic carbonyl or nitrile functionality. A shift of the fluoro- substituent in the terminal phenyl ring from *para*- to *meta*- (**7** and **29**, respectively) and *ortho*- positions (**8**) led to a loss of activity toward MMP-2 and MMP-13.

No compounds showed better potency against MMP-2 than the reference hit **BB 02231107** but almost all were more selective toward MMP-8. Concerning MMP-13 inhibition, the most promising substitutions in this series were *p*-(methylthio)phenyl compound **18** and heteroaryl analog **26** which were twice more active than **BB 02231107**. Compound **26** showed a non-selective inhibitory profile while **18** retained the selectivity to MMP-8.

The introduction of a substituent in R₃ is likely to gain the selectivity toward MMP-2 in most cases. This statement is substantiated by the *ortho*-nitro derivative **10** and the *ortho*-cyano derivative **13**. Preference for MMP-2 was also found for **9** despite no substituents at R₃. However, its activity was not promising, so the *ortho*-position was no longer explored. Given that all isatin derivatives from this scaffold (cluster A) with a substituent at *meta*- position (R₂) were inactive, no further efforts were undertaken in this direction.

Previously, we have reported the replacement of the phenyl moiety in the phenyl ring with thiophene, pyridine and pyrimidine moieties (Agamennone et al., 2016). Interestingly, the caboxymethylthiophene replacement (**26**) was promising for inhibition of MMP-2 and MMP-13. This compound as well as **18** were the most potent toward MMP-13. Unfortunately, **26** showed an undesirable activity toward MMP-8 leading to a loss of selectivity. No efforts to further explore this position were made. The replacement of CONHCH₃ group at R₁ posi-

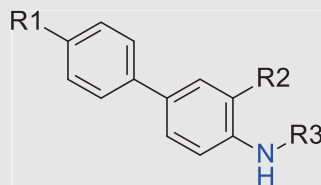
tion for NHAc (**5**) or CH₂NHAc (**17**) led to a total loss of activity. Therefore, the switch from the amide group for a bulkier substituent (**17** and **22**) is unworthy. Interestingly, the substitution at R₁ position with a hydrophilic moiety (**22**) abrogates the activity. These data strongly suggested that the substitution in the *para*-position (R₁) is the most promising for further exploration.

2.2. Synthesis and biological testing of Cluster B compounds

Unsymmetrical heteroaryl compounds can be used as potent MMP-12 inhibitors incorporating a thiophene template, an unusual central linker for MMP binding groups (Dublanche et al., 2005). In this case the biaryl moiety fits into the S1' pocket of the enzyme where binding interactions are mainly hydrophobic. Indeed, the core structures of thiophene and phenyl aromatic rings make hydrophobic contacts with Thr215, Tyr240 methylene, and His218 (Dublanche et al., 2005).

We investigated 'open' forms of isatin derivatives which are the analogs of biarylic compounds. Compound **30** was obtained by NaOH hydrolysis of the corresponding isatin **7** (Gérard et al., 2005). Esterification with methanol and ethanol led to compounds **31** and **32**, respectively. Compound **33** was obtained from methyl esterification of 2-amino-5-(*p*-tolyl) benzoic acid (Agamennone et al., 2016). Compound **34** was obtained via a Suzuki coupling reaction from the commercial (4-fluorophenyl)boronic acid and 4-bromoaniline (**34**; yield 64%). Compound **34** was acylated with acetylchloride to produce **35** in almost quantitative yield and **37** as a side product which was isolated and purified (details are available in Supplementary data). Compounds **30–36** with open isatin ring formed Cluster B.

Data in Table 2 showed that this modification was not promising as most of the tested compounds are inactive toward studied MMPs. On the other hand, compound **33** presented a good potency toward MMP-2 and MMP-13. However, **33** significantly inhibited MMP-8, an undesired feature for anticancer drug design (see Introduction). Therefore, no more compounds of this class were synthesized.

Table 2 Inhibition of MMP-2, MMP-8 and MMP-13 by Cluster B compounds 30–36.

ID	R ₁	R ₂	R ₃	Salt	IC ₅₀ , μM ^a		
					MMP-2	MMP-8	MMP-13
30, BB 0223070	F	COOH	H	–	56 ± 3	92 ± 4	> 100
31, BB 0305126	F	COOMe	H	–	> 100	> 100	> 100
32, BB 0305127	F	COOEt	H	–	> 100	> 100	> 100
BB 0223071 ^b	Me	COOH	H	–	> 100	> 100	79 ± 7
33, BB 0304409	Me	COOMe	H	–	11 ± 2	50 ± 5	3 ± 0.3
34, BB 0222486	F	H	H	–	> 100	> 100	> 100
35, BB 0305129	F	H	Ac	–	> 100	> 100	> 100
36, BB 0305128	F	H	HC(O)–	–	89 ± 26	> 100	> 100
NNGH ^c					0.0972 ± 0.0124	0.0327 ± 0.0019	0.0307 ± 0.0057

^a Data are mean ± SEM of at least three independent experiments in triplicate.

^b Published data (Agamennone et al., 2016).

^c Reference inhibitor: N-Isobutyl-N-(4-methoxyphenylsulfonyl)glycyl hydroxamic acid. Characterization of compounds is available from Supplementary data.

2.3. Synthesis and testing of Cluster C compounds

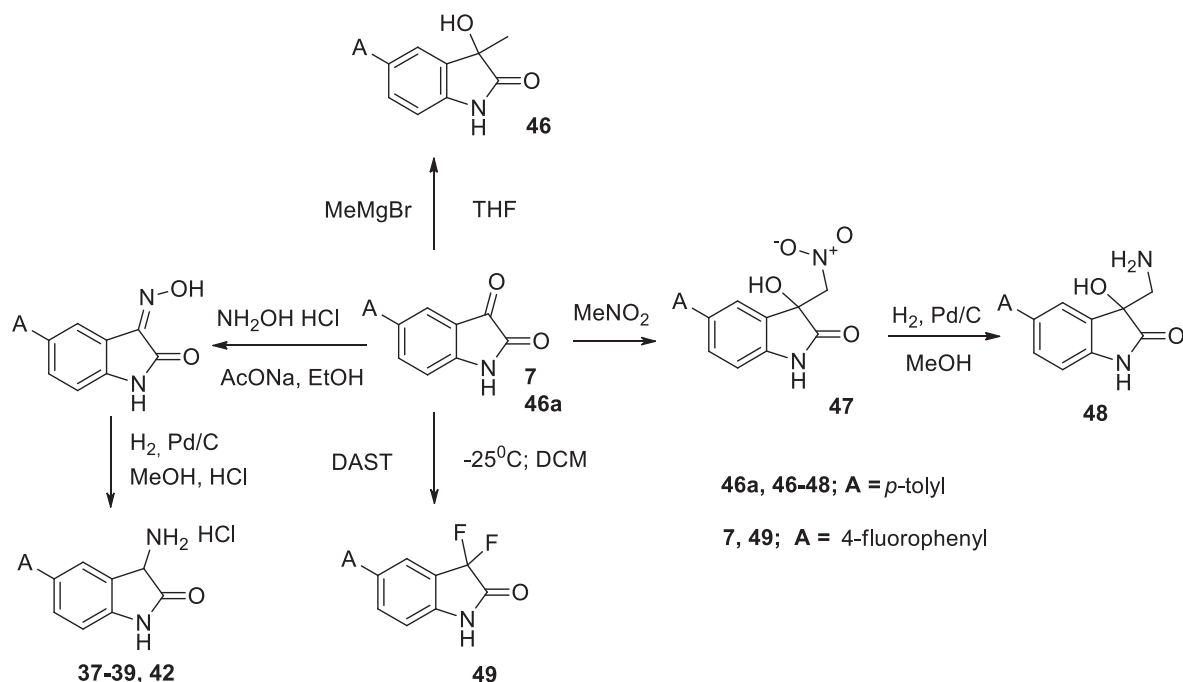
We have reported that replacement of one carbonyl group in (5-(*p*-tolyl)isatin for the amino group led to an increased potency against to enzymes MMP-2 and MMP-13 (Agamennone et al., 2016). Modification of carbonyl group as well as the use of simple reagents enables promising synthetic transformations of the isatin moiety. New compounds were synthesized as shown in Scheme 4. Derivatization of carbonyl groups in the isatin ring of monosubstituted isatins led to compounds 37–42 and 45–49 belonging to Cluster C (Scheme 3, Fig. 4 and Table 3). Compounds 37–39, 42 were synthesized in two steps by treatment of 5-(het)arylisatins with hydroxylamine hydrochloride in ethanol at reflux. The oximes were successfully hydrogenated to amines via traditional hydrogenation methods using molecular hydrogen and Pd/C (10%). The amide 40 and sulfamide 41 were obtained in 90% yield from 3-amino-5-(*p*-tolyl)indolin-2-one (Agamennone et al., 2016) by treatment of 3-amino-5-(*p*-tolyl)indolin-2-one or with acetyl chloride or methanesulfonyl chloride in CH₂Cl₂ in the presence of Et₃N at r.t. Compound 46 was prepared via a Grignard reaction starting from 5-*p*-tolyl-isatin (Agamennone et al., 2016). From the same substrate it was possible to prepare 47 via the Henry reaction (Holmquist et al., 2014) and its subsequent reduction with molecular hydrogen in the presence of Pd/C (10%). Compound 48 was obtained in 42% yield over two steps (Scheme 4).

Compound 49 was prepared by treatment of 7 with diethylaminosulfur trifluoride (DAST) in DCM at reflux (Scheme 3) (See Schemes 5–10 and Table 4).

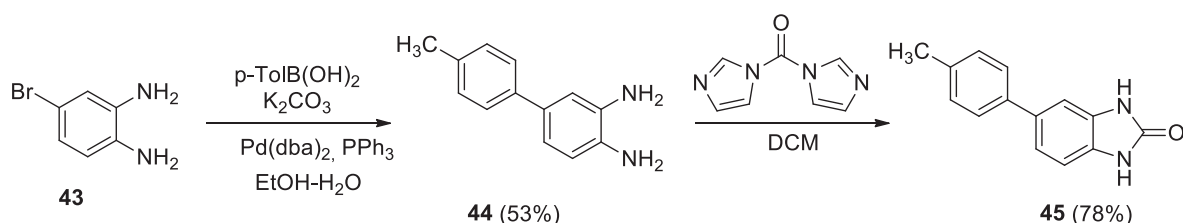
The 2(3H)-benzoimidazolone heterocycle gained attention due to its capability of mimicking a phenol or a catechol moiety in a metabolically stable template (Poupaert et al., 2005) and therefore factored in the design of 45. Compound 45 was synthesized as shown in Scheme 4. The benzoimidazolone ring was prepared from the appropriate 4'-methyl-[1,1'-biphenyl]-3,4-diamine (44) by treatment with 1,1'-carbonyldiimidazole (CDI) in THF at r.t. (Nakao et al., 2014).

Replacement of one carbonyl group in isatin with an amino group led to a twofold improvement of MMP-13 inhibition activity (mean IC₅₀ = 3.4 μM for 37 compared to mean IC₅₀ = 6.2 μM for BB 0223107) and improved selectivity to MMP-8. This observation is in accord with data on *p*-tolyl isatin derivative 46a and the corresponding 3-amino-5-(*p*-tolyl)indolin-2-one (Agamennone et al., 2016) (IC₅₀ = 16 μM and 3.4 μM toward MMP-13 and MMP-2, respectively). This new scaffold may represent a good alternative to the isatin group, since isatin based compounds may have off-target effects (Justo et al., 2016; Pakravan et al., 2013). Indeed, the isatin scaffold is filtered through PAINS produced alert (Baell and Holloway, 2010) whereas the new scaffold is not.

It is also important to note that, as a result of the synthesis of Cluster C, we obtained only the racemic forms of 5-(het)aryl-3-aminoindoles (37–42). Separation of enantiomers



Scheme 3 Synthetic routes for compounds 37–39, 42, 46–49. Details are available in *Supplementary data*. Preparation and characterization of **46a** is described in [Agamennone et al. \(2016\)](#).



Scheme 4 Synthesis of benzoimidazolone **45**.

and testing their activities are under way. The speculation that one of the individual enantiomers may have a high inhibitory potency is not excluded.

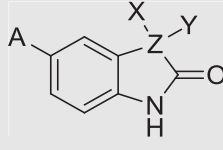
2.4. Molecular modeling

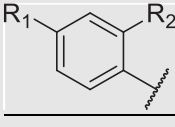
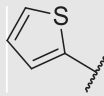
To get insight into the binding mode of the studied fragments, a structure-based computational analysis was carried out using the Schrodinger Suite 2019–4 ([Schrödinger, 2019](#)). All isatin-based ligands including the published ones ([Agamennone et al., 2016](#)) were prepared using the cxcalc tool ([Chemaxon, 2020](#)) and docked into the binding site of MMP-2, MMP-8 and MMP-13. Three dimensional structures of enzymes were selected through cross-docking procedure ([Ammazzalorso et al., 2016](#)).

In the previous article ([Agamennone et al., 2016](#)), the structure-based analysis carried out on MMP-2 and MMP-13 catalytic sites, suggested a putative binding mode of isatin derivatives. In the present study, focusing on MMP-2 binding, we examined the binding of these compounds taking into account the flexibility of the target protein and the presence of water molecules (see *Supplementary data*). The application of the Induced fit protocol to account for flexibility did not

improve the results while inclusion of water molecules around the ligands afforded a good discrimination between active and inactive compounds for MMP-2 (ROC = 0.74; AUC = 0.67; Table S1 in *Supplementary data*).

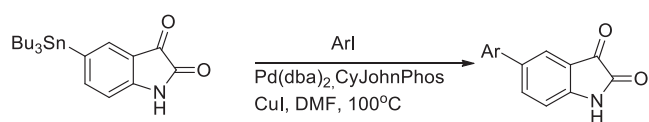
The analysis of binding geometries confirmed that all fragments occupied the S1' site in the three enzymes and no ligand is able to coordinate the catalytic zinc ion. In particular, class A ligands bind as already observed in the previous work. In particular, the binding mode of studied isatins into MMP-2 is pretty well conserved. Ligands **7** and **26** occupy the enzyme catalytic site as already observed for reference compound and forming a H-bond network between the isatin NH and the Glu202 carboxylic function and the carbonyl oxygen in **2** with Leu164 and Ala165 NH ([Fig. 5 A, B](#)). In MMP-13, the longer S1' site allows the ligand's shifting toward the bottom of the specificity site, maintaining the H-bond contact between the isatin NH and Phe117 C = O. The acceptor group in the *para* position of the distal aromatic ring establishes a polar contact with Lys228 side chain ([Fig. 5 C, D](#)). A similar result has been obtained from docking into the MMP-8 site where the presence of Arg222 favors the binding of ligands with a H-bond acceptor group on the distal ring (**26**) providing an explanation of the observed activity for this ligand. The isatin ring is

Table 3 Inhibition of MMP-2, MMP-8 and MMP-13 by Cluster C compounds 37–42, 45–49.


Compound ID	A	Z	Y	X	Salt	IC ₅₀ (μM) ^a	MMP-2	MMP-8	MMP-13	
	 Hetero									
	R ₁	R ₂								
37, BB 0270669	–COOMe	H	–	C	H	NH ₂	HCl	14 ± 1	> 100	3 ± 1
38, BB 0300738	–CONHMe	H	–	C	H	NH ₂	HCl	31 ± 4	> 100	75 ± 13
39, BB 0300736	H	Cl	–	C	H	NH ₂	HCl	20 ± 3	> 100	13 ± 4
40, BB 0300740	Me	H	–	C	H	NHAc	HCl	> 100	> 100	20 ± 8
41, BB 0300744	Me	H	–	C	H	NHSO ₂ Me	–	> 100	> 100	87 ± 2
42, BB 0300737	–	–		C	H	NH ₂	HCl	> 100	> 100	25 ± 4
45, BB 0300745	Me	H	–	N	H	–	–	> 100	> 100	> 100
46, BB 0300751	Me	H	–	C	OH	Me	–	> 100	> 100	> 100
47, BB 0304411	Me	H	–	C	OH	CH ₂ NO ₂	–	> 100	> 100	> 100
48, BB 0304410	Me	H	–	C	OH	CH ₂ NH ₂	–	> 100	> 100	> 100
49, BB 0305125	F	H	–	C	F	F	–	> 100	> 100	> 100
NNGH ^b								0.0972 ± 0.0124	0.0327 ± 0.0019	0.0307 ± 0.0057

^a Data represent mean ± SEM of at least three independent experiments in triplicate.

^b Reference inhibitor: N-Isobutyl-N-(4-methoxyphenylsulfonyl)glycyl hydroxamic acid.

**Scheme 5** Synthesis of 5-Arylisatins.

H-bonded to Leu160 NH, Ala161 NH and Glu198 COOH (Fig. 5 E).

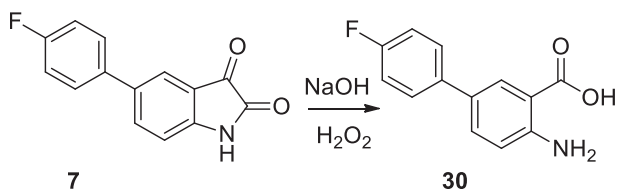
Class B ligands, represented by compound **33**, present a similar binding geometry in all studied MMPs, with the aniline NH₂ forming H-bond interactions alternatively with Glu202 (MMP-2) and Ala161/165C=O (MMP-8 and MMP-13), while the distal phenyl ring gives a π-π contact with His201 (MMP-2 numbering, Fig. 6).

Benzimidazolone derivatives can invert their binding orientation in the S1' site with the heterocyclic ring occupying

the bottom of the S1' site in both MMP-8 and MMP-13, while it retains the same orientation in the MMP-2.

In order to verify the validity of this binding mode, a MD run was carried out on the best ligand (**37**) in complex with MMP-2. The ligand maintained its position with conserved interactions (π-π stacking with His201 and H-bond to Glu202 in ~90% of the trajectory; see Supporting Information) along the simulation, thereby confirming the reliability of the observed binding mode. The main difference with respect to the docked pose was the insertion of a bridge water molecule between the carbonyl of 3-aminoindolin-2-one in the position 2 and Leu164 NH (Fig. 7A).

Binding in the MMP-13 active site differed from that in the MMP-2 binding site, with the ligand flipped toward the bottom of the S1' site. Interestingly, the most active ligand of this series (**37**) orients the -COOMe substituent toward the top of the S1' site with the distal ring forming a π-π stacking with His201, while the heterocyclic ring forms a network of



Scheme 6 Synthesis of compound 30.

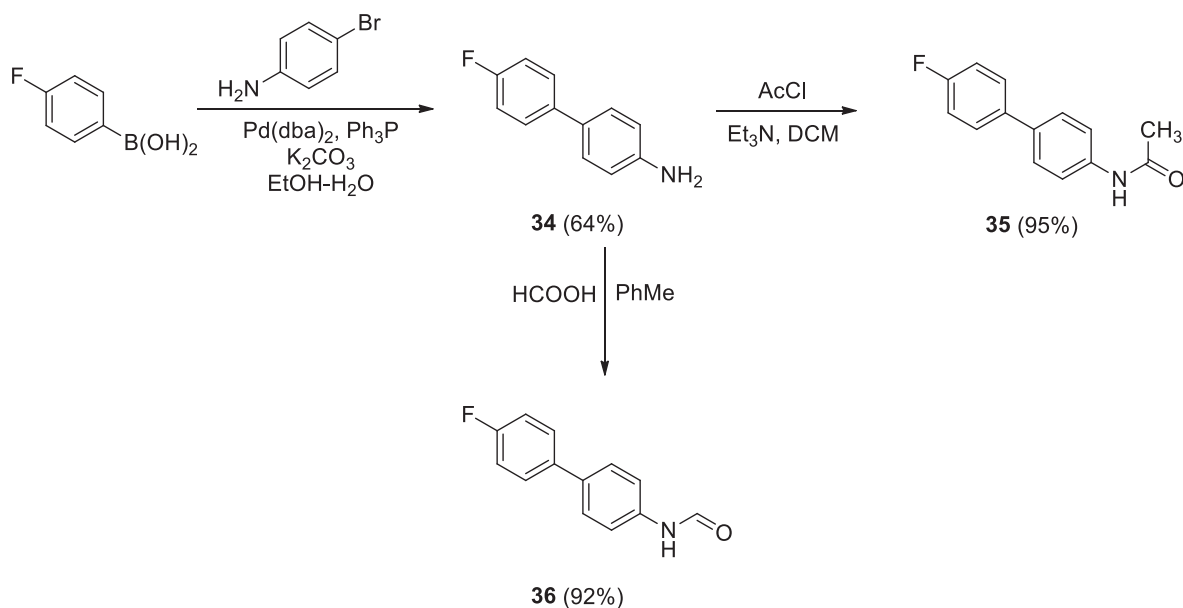
H-bonds with Thr224 OH, Pro215 C=O and Ile222 C=O, (Fig. 7B).

Docking analysis of compound **37** on MMP-8 reported a binding geometry slightly different from MMP-2 but with good docking scores. These results did not help explaining the selectivity toward MMP-8, as the inactive ligands achieved very high scores. Therefore, to get an idea in regard to MMP-8 preference, the docked complex MMP-8:**37** was submitted to a

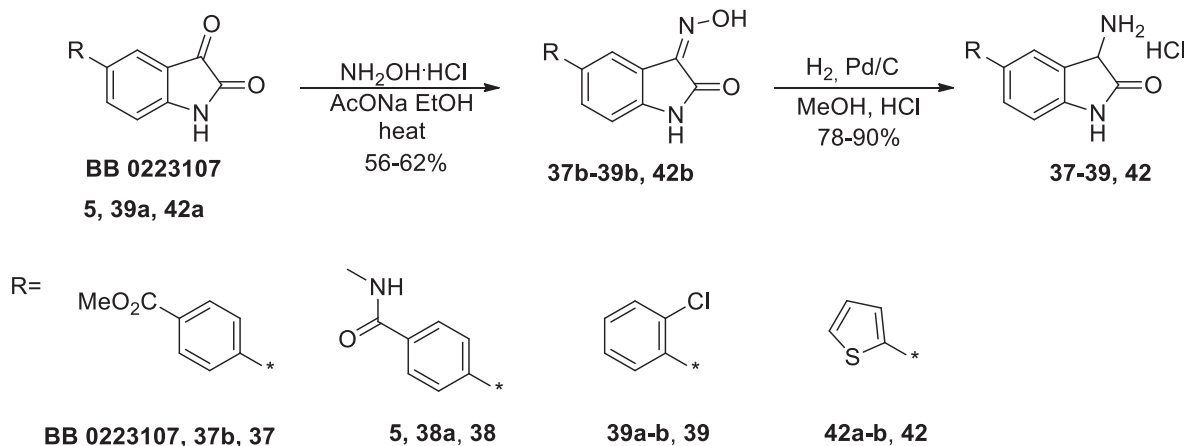
20 ns MD simulation. The binding geometry of **37** was stable during all the trajectory although Arg222 side chain was displaced from its conserved water-mediated interaction with Pro211. The subsequent destabilization of the protein can contribute to the lack of inhibitory potency of this ligand series toward MMP-8.

3. Conclusion

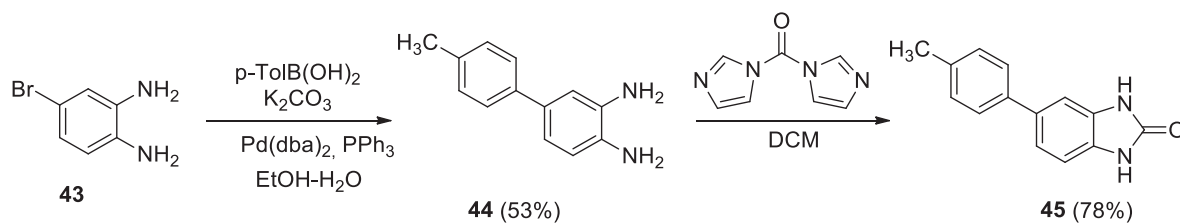
We performed a scaffold hopping procedure (Fig. 8) by changing tentatively PAINS alerted isatin scaffold for methyl 4-(3-amino-2-oxoindolin-5-yl)benzoate hydrochloride. Compound **37**, while losing the inhibitory potency toward MMP-13 (mean $IC_{50} = 13 \mu\text{M}$ for **37** vs $4 \mu\text{M}$ for the reference **BB 0223107**) showed, instead, a twofold increase of the activity against MMP-2 (**37** = $3 \mu\text{M}$ vs **BB 0223107** = $6 \mu\text{M}$) and an improved selectivity to MMP-8 (**BB 0223107** = $57 \mu\text{M}$ vs **37** > $100 \mu\text{M}$).



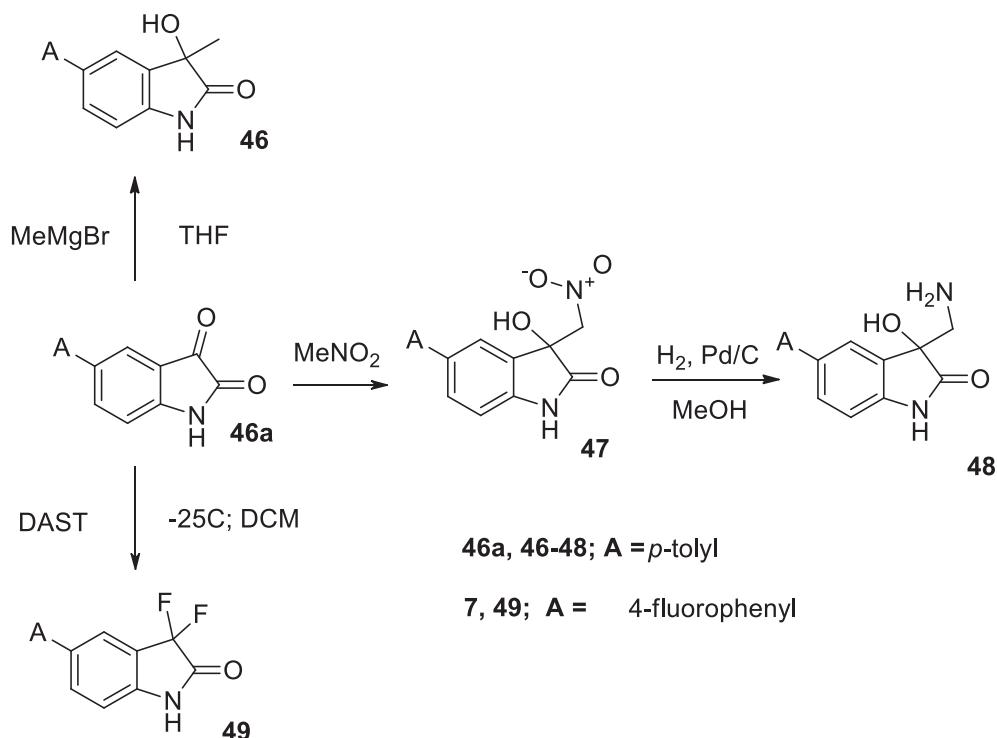
Scheme 7 Scheme of synthesis of compounds 35 and 36.



Scheme 8 Scheme of synthesis of compounds 37–39, 42.



Scheme 9 Scheme synthesis of compound 45.



Scheme 10 Scheme of synthesis of compounds 46–49. Synthesis of 46a and its characterization described in a previous work (Agamennone et al., 2016).

Another advantage of the new scaffold is its versatile amino moiety prone to functionalization. This moiety deserves further investigation in the coupling reactions or stereoselective reductive amination amenable for automated HTC procedures. Identification of the new scaffold represents a starting point for development of selective non-zinc-binding inhibitors (compound **37** as a prototype) directed toward the tumor progression related MMP-2 and MMP-13 and sparing the anti-cancer MMP-8 enzyme.

4. Materials and methods

4.1. Materials

NMR spectra were acquired on Bruker Avance 400 spectrometer at room temperature; the chemical shifts δ were measured in ppm with respect to solvent (1H: CDCl_3 , $\delta = 7.28$ ppm; DMSO d_6 : $\delta = 2.50$ ppm; ^{13}C : CDCl_3 , $\delta = 77.2$ ppm; DMSO d_6 : $\delta = 39.5$ ppm). Splitting patterns are designated as s, singlet; d, doublet; t, triplet; q, quadruplet; quint, quintet; m, multiplet; dd, double doublet, br., broad. Coupling con-

stants (J) are given in Hertz. The structures of synthesized compounds were elucidated with the aid of ^1H , ^{13}C spectroscopy. Infrared spectra were recorded on Thermo Nicolet IR-200 in KBr, nujol or neat. High-resolution mass spectra (HRMS) were carried out the Thermo Scientific LTQ Orbitrap instrument using nano-electrospray ionization (nano-ESI). Low-resolution mass spectra were on Finnigan MAT mass spectrometer using electron ionization (direct inlet) and an ITD-700 detector with the ionizing electron energy being 70 eV and the mass range being m/z 35–400. Elemental analysis was performed on EURO EA CHN Elemental Analyzer. The melting points (m.p.) were measured in open capillaries and presented without correction.

4.2. Synthetic protocols and compound characterizations

4.2.1. General procedure (GP1) for the synthesis of 5-Arylisatins

5-Bromoisatin (2.26 g, 10.0 mmol) was suspended in a mixture of ethanol (10 mL) and water (10 mL) under constant flow of nitrogen. K_2CO_3 (4.14 g, 30.0 mmol, 3 equiv) was added and

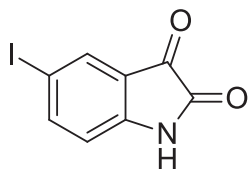
Table 4 Enrichment values obtained ranking compounds on the basis of the docking score for different docking procedure applied to MMP-2 receptor. Compounds are considered active if their $pIC_{50} \geq 4.5$.

Docking protocol	ROC	RIE	AUC
SP	0.59	0.7	0.57
XP	0.60	1.38	0.57
Induced fit	0.61	1.07	0.57
SP with water molecules	0.72	2.54	0.66
XP with water molecules	0.74	2.12	0.67

the mixture was heated at reflux till the solution become almost colorless (5–10 min). The solution was cooled to ambient temperature and the corresponding arylboronic acid (13.0 mmol, 1.3 equiv) added, followed by the addition of Pd(dppf)Cl₂ (73 mg, 1 mol. %). The reaction mixture was heated at reflux for 8 h, cooled to ambient temperature and acetic acid (100 mL) was added. The resulting mixture was heated at reflux for 10 min. In case of precipitate formation after cooling, then it was filtered and recrystallized one more time from and hot solution of acetic acid, filtered and the catalyst residue removed. In all the other cases, the acetic acid was diluted with water (~200 mL) and the product was extracted with ethyl acetate (3x100 mL). The combined organic layers were dried over Na₂SO₄, filtered and evaporated. The residue was purified via chromatography (eluent hexanes/EtOAc, 1:1, 0:1). If necessary, the product was further recrystallized from ethanol.

4.2.2. General procedure (GP2) for the synthesis of 5-Arylisatins

5-Iodo-indole-2,3-dione (1)



5-Iodo-indole-2,3-dione (**1**) was prepared according to the modified literature procedure (Bass, 2017). ICl (16.2 g, 10.0 mmol, 1 equiv) was portion wise added to 1 M aqueous solution of KCl (22.3 g, 30.0 mmol, 3 equiv). The reaction mixture was stirred half of a hour, then 1 M methanol solution of isatin was added (14.7 g, 10.0 mmol, 1 equiv). The reaction mixture was stirred for 8 h, then filtered off.

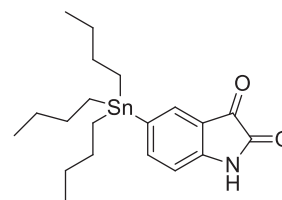
Compound **1** was synthesized according to the literature procedure (Emilie et al., 2015) from *p*-iodoisatinacetanilide (22.0 g, 75.9 mmol). The resulting solution was heated in H₂SO₄ at 80 °C for 15 min. After cooling to room temperature and then to 0 °C, the reaction mixture was poured on crushed ice and stirred at 0 °C for 2 h. The orange formed precipitate was filtered, washed with water and dissolved in a 10% aqueous sodium hydroxide solution (100 mL), previously warmed to 60 °C. Acetic acid was then added (16.5 mL), and the solution was heated at 60 °C for 30 min. After cooling to room temperature and then to 0 °C,

the formed precipitate was filtered, washed with water and dried under *vacuum* to give 5-iodoisatin (17.6 g, 85%); m.p. = 272–274 °C

Spectral data are well consistent with the published ones (Emilie et al., 2015; Iara et al., 2019)

¹H NMR (DMSO *d*₆), δ ppm: 6.76 (d, 1H), 7.73 (d, *J* = 1.6 Hz, 1H), 7.86 (dd, *J* = 8.2, 1.8 Hz, 1H), 11.19 (s, 1H).

5-Tributhylstannyl-indole-2,3-dione (2)



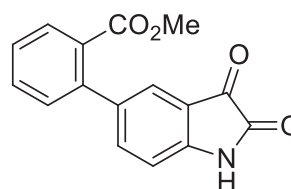
Compound **1** (5.46 g, 2.00 mmol, 1 equiv) was dissolved in DMF (50 mL, 0.2 M) under an argon atmosphere, followed by the addition of triphenylphosphine (262 mg, 1.00 mmol) and Pd(dba)₂ (287 mg, 0.50 mmol). The reaction was stirred for 15 min followed by the addition of bis-tributyltin (17.75 g, 3.00 mmol, 1.5 equiv). The resulting mixture was stirred at 100 °C for 10 h, poured into water and extracted with ethyl acetate. The organic layer was dried over sodium sulfate, filtered and evaporated under reduced pressure. The obtained residue was purified via column chromatography. M = 1.56 g. Yield = 27% Spectral data are well consistent with the published ones (Natsumi et al., 2018)

¹H NMR (CDCl₃), δ ppm: 0.86–0.93 (m, 11H), 1.04–1.10 (m, 5H), 1.28–1.37 (m, 8H), 1.48–1.55 (m, 3H), 6.92 (d, *J* = 7.5 Hz, 1 H), 7.53–7.73 (m, 2 H), 8.57 (br.s., 1 H).

Compound **2** (1.5 equiv) was dissolved in DMF (1 M) under an argon atmosphere and the corresponding haloarene was added (1 equiv). The resulting mixture was stirred for 5 min, then Pd(dba)₂ (2 %), CyJohnPhos (4%) and CuI (4%) were added. The reaction was stirred at 100 °C for 10 h, then poured into water and extracted with ethyl acetate. The organic layer was dried over sodium sulfate, filtered and evaporated under reduced pressure. The resulting residue purified by column chromatography.

4.2.3. Characterization of 5-Arylisatin compounds

Methyl 2-(2,3-dioxindolin-5-yl)benzoate (**3**, BB 0305124) was synthesized according to the GP2 from **2** (436 mg, 1.00 mmol). Yield: 12%, M = 28 mg. Red solid, m.p. = 216–218 °C



¹H NMR (DMSO *d*₆), δ ppm: 3.63 (s, 3H), 6.96 (d, *J* = 8.07 Hz, 1H), 7.36–7.45 (m, 2H), 7.50 (t, *J* = 7.27 Hz, 2H), 7.63 (t, *J* = 7.27 Hz, 1H), 7.79 (d, *J* = 7.58 Hz, 1H), 11.14 (br. s., 1H).

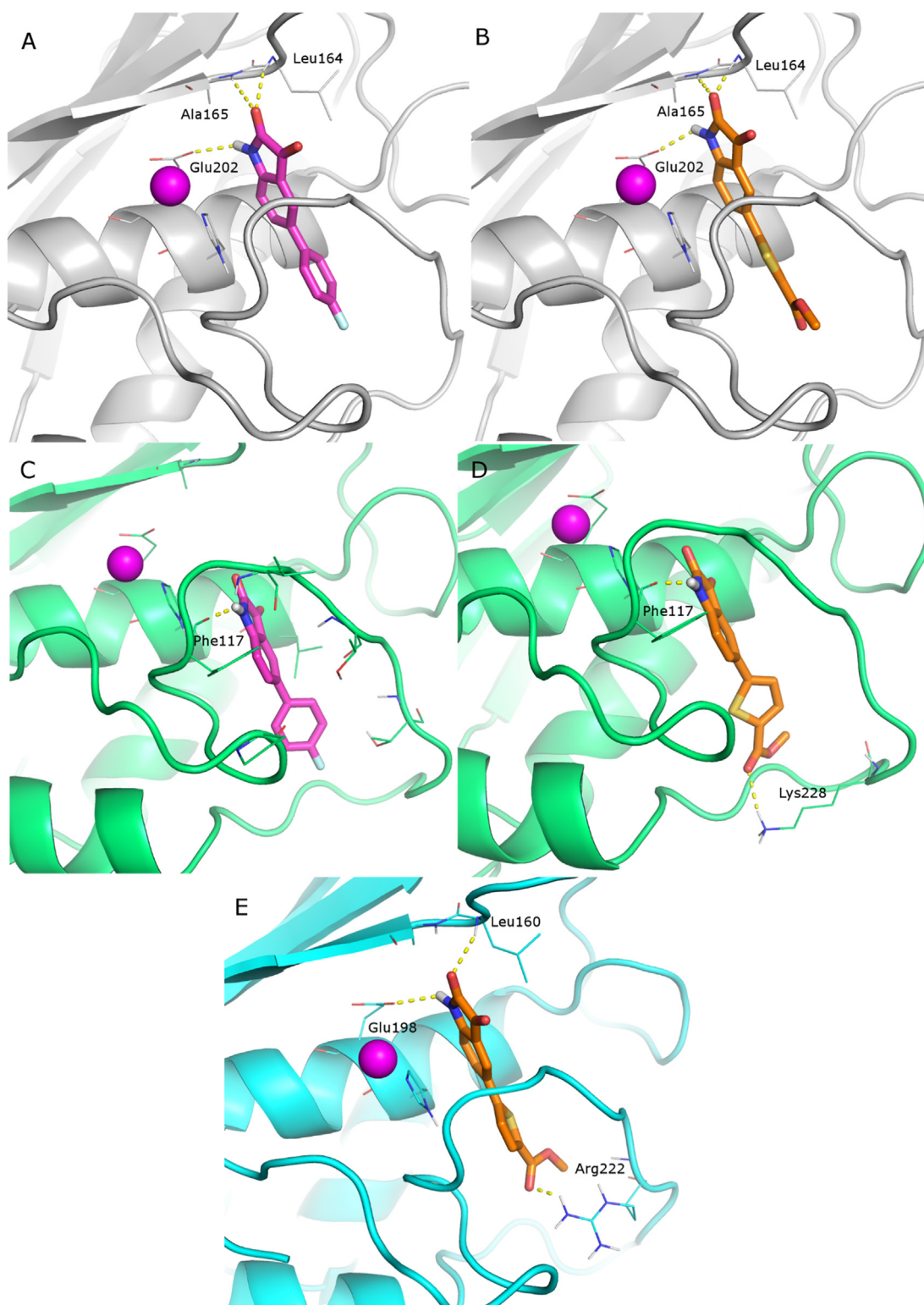


Fig. 5 Docked poses of compounds 7 (stick, pink C atoms) and 26 (stick, orange C atoms) in: (A and B) MMP-2 binding site (grey cartoon); (C and D) MMP-13 binding site (green cartoon); (E) MMP-8 binding site (cyan cartoon). The catalytic zinc ion is represented as a magenta sphere, H-bonds are rendered as yellow dashed lines.

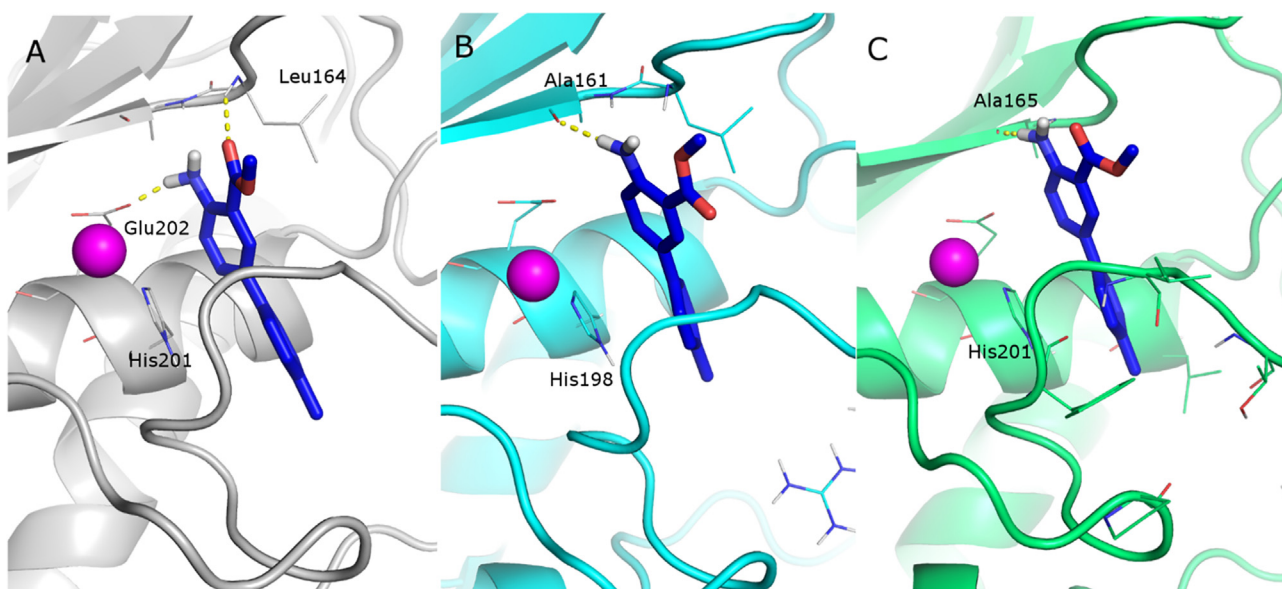


Fig. 6 Docked poses of compound 33 (stick, blue C atoms) in: (A) MMP-2 binding site (grey cartoon); (B) MMP-13 binding site (green cartoon); (C) MMP-8 binding site (cyan cartoon). The catalytic zinc ion is represented as a magenta sphere, H-bonds are rendered as yellow dashed lines.

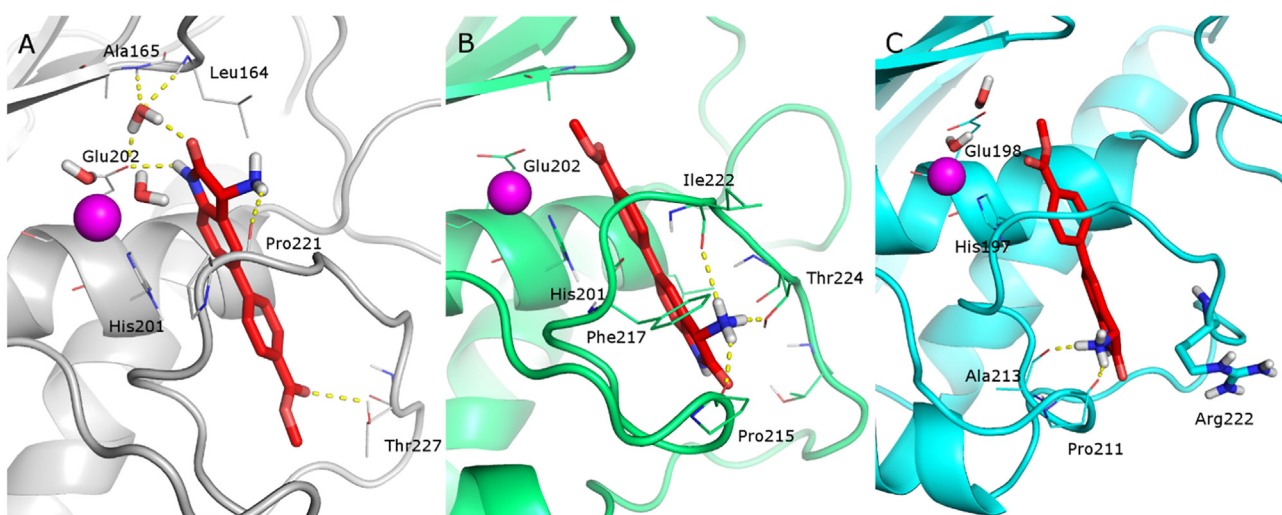


Fig. 7 Binding geometry of compound 37 (stick, red C atoms) in: (A) MMP-2 binding site (grey cartoon) as the most representative of MD calculation; (B) MMP-13 binding site (green cartoon) after docking; (C) MMP-8 binding site (cyan cartoon) as the most representative of MD calculation. The catalytic zinc ion is represented as a magenta sphere, H-bonds are rendered as yellow dashed lines.

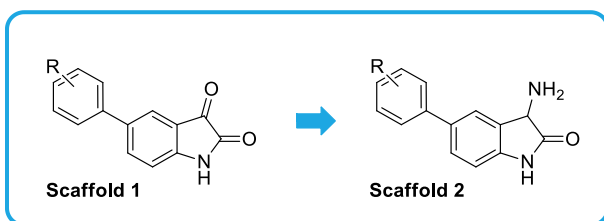


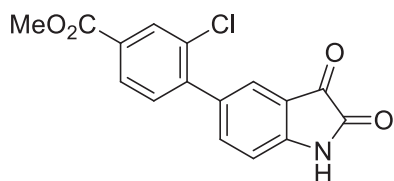
Fig. 8 Scheme of the scaffold shift.

^{13}C NMR (DMSO d_6), δ ppm: 52.1, 112.0, 117.7, 123.9, 127.8, 129.7, 130.2, 130.5, 131.8, 135.1, 138.2, 140.0, 149.9, 159.5, 168.1, 184.3.

IR ν_{max} (nujol): 2964, 2949, 2929, 2906, 2846, 1726, 1618, 1464, 1377, 719 cm^{-1} .

HRMS (ESI) m/z : $\text{C}_{16}\text{H}_{12}\text{NO}_4$ $[\text{M} + \text{H}]^+$, 282.2628; Found 282.2627.

Methyl 3-chloro-4-(2,3-dioxindolin-5-yl)benzoate (**4**, BB 0305116) was synthesized according to the GP2 from **2** (436 mg, 1.00 mmol). Yield: 58%, M = 180 mg. Red solid, m.p. = 242–244 $^{\circ}\text{C}$



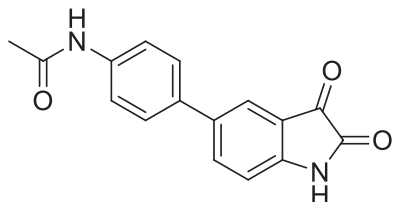
$^1\text{H NMR}$ (DMSO d_6), δ ppm: 3.89 (s, 3H), 7.03 (d, $J = 8.19$ Hz, 1H), 7.55–7.63 (m, 2H), 7.71 (dd, $J = 8.13$, 1.90 Hz, 1H), 7.96 (dd, $J = 8.01$, 1.65 Hz, 1H), 8.04 (d, $J = 1.47$ Hz, 1H), 11.22 (br. s., 1H).

$^{13}\text{C NMR}$ (DMSO d_6), δ ppm: 52.6, 112.2, 117.8, 125.1, 128.2, 130.4, 131.8, 139.0, 142.7, 150.6, 159.5, 164.8, 184.0.

IR ν_{max} (nujol): 3271, 2920, 2856, 1766, 1734, 1716, 1624, 1462, 1296 cm^{-1} .

HRMS (ESI) m/z : $\text{C}_{16}\text{H}_{11}\text{ClNO}_4$ $[\text{M} + \text{H}]^+$, 316.0371; Found 316.0369.

N-(4-(2,3-Dioxindolin-5-yl)phenyl)acetamide (5, BB 0304038) was synthesized according to the GP2 from 2 (436 mg, 1.00 mmol). Yield: 39%, M = 110 mg. Red solid, m.p. = 268–270 °C



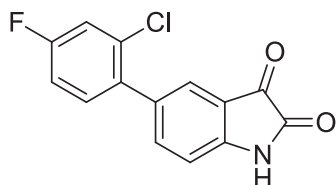
$^1\text{H NMR}$ (DMSO d_6), δ ppm.: 2.06 (s, 3H), 6.97 (d, $J = 8.19$ Hz, 1H), 7.53–7.61 (m, 2H), 7.62–7.68 (m, 2H), 7.73 (d, $J = 1.71$ Hz, 1H), 7.87 (dd, $J = 8.25$, 1.89 Hz, 1H), 10.02 (s, 1H), 11.10 (s, 1H).

$^{13}\text{C NMR}$ (DMSO d_6), δ ppm: 24.1, 112.6, 118.4, 119.3, 122.0, 126.4, 133.2, 134.6, 135.9, 138.8, 149.5, 159.6, 168.4, 184.4.

IR ν_{max} (nujol): 2858, 1952, 1754, 1624, 1604, 1541, 1443, 1377, 1306 cm^{-1} .

HRMS (ESI) m/z : $\text{C}_{16}\text{H}_{13}\text{N}_2\text{O}_3$ $[\text{M} + \text{H}]^+$, 281.0921; Found 281.0922.

5-(2-Chloro-4-fluorophenyl)indoline-2,3-dione (6, BB 0305115) was synthesized according to the GP2 from 2 (436 mg, 0.1.00 mmol). Yield: 54%, M = 149 mg. Red solid, m.p. = 208–210 °C



$^1\text{H NMR}$ (DMSO d_6), δ ppm: 7.00 (d, $J = 8.07$ Hz, 1H), 7.31 (td, $J = 8.28$, 2.26 Hz, 1H), 7.48 (dd, $J = 8.13$, 6.79 Hz, 1H), 7.52 (s, 1H), 7.57 (dd, $J = 8.93$, 2.45 Hz, 1H), 7.63 (d, $J = 8.19$ Hz, 1H), 11.17 (s, 1H).

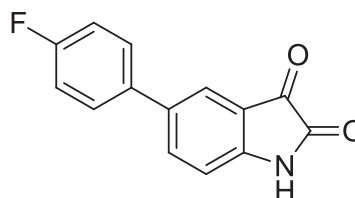
$^{13}\text{C NMR}$ (DMSO d_6), δ ppm: 112.1, 114.8 (d, $J = 20.9$ Hz), 117.1 (d, $J = 24.9$ Hz), 117.8, 125.2, 132.1,

132.3, 132.7 (d, $J = 8.8$ Hz), 132.8, 134.9, 139.2, 150.2, 159.5, 161.2 (d, $J = 248.2$ Hz), 184.1.

IR ν_{max} (nujol): 2970, 2901, 2883, 2817, 1711, 1673, 1435, 1371, 1208 cm^{-1} .

HRMS (ESI) m/z : $\text{C}_{14}\text{H}_8\text{ClFNO}_2$ $[\text{M} + \text{H}]^+$, 276.0222; Found 276.0221.

5-(4-Fluorophenyl)indoline-2,3-dione (7, BB 0223093) was synthesized according to the GP1 from 1 (273 mg, 1.00 mmol). Yield 76%, M = 183 mg. Red solid, m.p. = 220–223 °C. Spectral data are well consistent with the published ones (Wang et al., 2012).



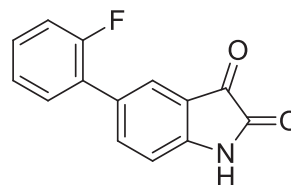
$^1\text{H NMR}$ (DMSO d_6), δ ppm: 7.03 (d, $J = 8.19$ Hz, 1H), 7.27 (t, $J = 8.80$ Hz, 2H), 7.70 (dd, $J = 8.74$, 5.44 Hz, 2H), 7.74 (d, $J = 1.96$ Hz, 1H), 7.87 (dd, $J = 8.2$, 2.0 Hz, 1H), 11.13 (bs, 1H).

$^{13}\text{C NMR}$ (DMSO d_6), δ ppm: 112.9, 115.8 (d, 2C, $J = 21.2$ Hz), 118.4, 122.4, 128.3 (d, 2C, $J = 8.1$ Hz), 133.8, 135.3 (d, $J = 2.9$ Hz), 135.3, 136.4, 150.4, 159.7, 160.9 (d, $J = 244.4$ Hz), 173.5, 184.7.

IR ν_{max} (nujol): 3237, 1769, 1738, 1728, 1716, 1620, 1465, 1456, 1201, 836, 741 cm^{-1} .

HRMS (ESI) m/z : $\text{C}_{14}\text{H}_8\text{FNO}_2$ $[\text{M} + \text{Na}]^+$, 264.0431; Found 264.0430.

5-(2-Fluorophenyl)indoline-2,3-dione (8, BB 0223954) was synthesized according to the GP1 from 1 (273 mg, 1.00 mmol). Yield 47%, M = 114 mg. Red solid, m.p. = 212–214 °C



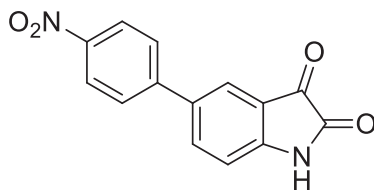
$^1\text{H NMR}$ (DMSO d_6), δ ppm: 7.01 (d, $J = 8.27$ Hz, 1H), 7.20–7.34 (m, 2H), 7.40 (d, $J = 6.04$ Hz, 1H), 7.50 (t, $J = 7.63$ Hz, 1H), 7.61 (br. s., 1H), 7.74 (d, $J = 7.95$ Hz, 1H), 11.17 (br. s., 1H).

$^{13}\text{C NMR}$ (DMSO d_6), δ ppm: 112.5, 116.1 (d, $J = 22.7$ Hz), 118.1, 124.6, 124.6 (d, $J = 2.9$ Hz), 125.0 (d, $J = 2.9$ Hz), 126.8 (d, $J = 12.8$ Hz), 129.5, 129.7 (d, $J = 8.1$ Hz), 130.3, 138.5, 150.2, 159.1 (d, $J = 245.$, 159.5, 184.2.

IR ν_{max} (nujol): 3237, 1769, 1738, 1728, 1716, 1620, 1465, 1456, 1201, 836, 741 cm^{-1} .

HRMS (ESI) m/z : $\text{C}_{14}\text{H}_8\text{FNO}_2$ $[\text{M} + \text{H}]^+$, 242.0612; Found 242.0612.

5-(4-Nitrophenyl)indoline-2,3-dione (9, BB 0305121) was synthesized according to the **GP2** from **2** (436 g, 1.00 mmol). Yield: 43%, M = 115 mg. Red solid, m.p. = 238–240 °C



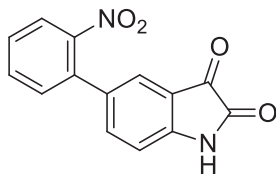
$^1\text{H NMR}$ ($\text{DMSO } d_6$), δ ppm: 7.04 (d, J = 8.19 Hz, 1H), 7.89–7.99 (m, 3H), 8.00–8.06 (m, 1H), 8.26 (d, J = 8.68 Hz, 2H), 11.25 (s, 1H).

$^{13}\text{C NMR}$ ($\text{DMSO } d_6$), δ ppm: 118.7, 123.2, 124.1, 127.3, 132.2, 136.9, 145.2, 146.4, 151.1, 159.6, 163.2, 171.2, 184.0.

IR v_{max} (nujol): 2803, 1758, 1703, 1613, 1567, 1450, 1381, 1291, cm^{-1} .

HRMS (ESI) m/z : $\text{C}_{14}\text{H}_9\text{N}_2\text{O}_4$ [$\text{M} + \text{H}$] $^+$, 269.2243; **Found** 269.2249.

5-(2-Nitrophenyl)indoline-2,3-dione (10, BB 0305122) was synthesized according to the **GP2** from **2** (436 mg, 1.00 mmol). Yield: 34%, M = 91 mg. Red solid, m.p. = 25 0–252 °C.



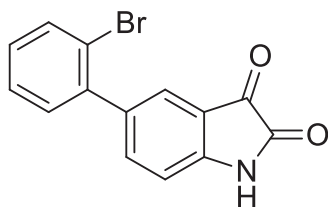
$^1\text{H NMR}$ ($\text{DMSO } d_6$), δ ppm: 6.99 (d, J = 8.19 Hz, 1H), 7.50 (s, 1H), 7.56 (t, J = 8.25 Hz, 2H), 7.64 (t, J = 7.76 Hz, 1H), 7.77 (t, J = 7.58 Hz, 1H), 8.02 (d, J = 8.07 Hz, 1H), 11.18 (s, 1H).

$^{13}\text{C NMR}$ ($\text{DMSO } d_6$), δ ppm: 112.5, 118.1, 123.8, 124.4, 129.2, 131.5, 131.9, 133.2, 133.8, 137.7, 148.5, 150.5, 159.4, 184.0.

IR v_{max} (nujol): 3237, 1769, 1738, 1728, 1716, 1620, 1465, 1456, 1201, 836, 741 cm^{-1} .

HRMS (ESI) m/z : $\text{C}_{14}\text{H}_9\text{N}_2\text{O}_4$ [$\text{M} + \text{H}$] $^+$, 269.2243; **Found** 269.2245.

5-(2-Bromophenyl)indoline-2,3-dione (11, BB 0305120) was synthesized according to the **GP2** from **2** (436 mg, 1.00 mmol). Yield: 59%, M = 180 mg. Red solid, m.p. = 2 54–256 °C



$^1\text{H NMR}$ ($\text{DMSO } d_6$), δ ppm: 7.00 (d, J = 8.07 Hz, 1H), 7.29–7.35 (m, 1H), 7.38–7.43 (m, 1H), 7.43–7.53 (m, 2H),

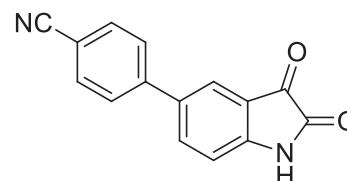
7.62 (d, J = 8.07 Hz, 1H), 7.74 (d, J = 8.93 Hz, 1H), 11.17 (s, 1H).

$^{13}\text{C NMR}$ ($\text{DMSO } d_6$), δ ppm: 112.0, 117.6, 121.8, 125.0, 128.2, 129.7, 131.3, 133.1, 134.8, 139.2, 140.3, 150.1, 159.5, 184.1.

IR v_{max} (nujol): 3280, 2611, 1822, 1719, 1694, 1627, 1500, 1427 cm^{-1} .

HRMS (ESI) m/z : $\text{C}_{14}\text{H}_9\text{BrNO}_2$ [$\text{M} + \text{H}$] $^+$, 303.1228; **Found** 303.1226.

4-(2,3-Dioxindolin-5-yl)benzotrile (12, BB 0223114) was synthesized according to the **GPI** from **1** (273 mg, 1.00 mmol). Yield: 21%, M = 52 mg. Red solid, m.p. = 200–202 °C. Spectral data are well consistent with the published ones (Wang et al., 2012).



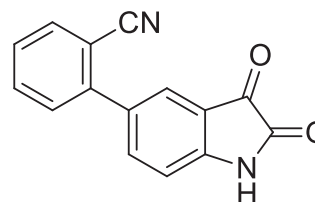
$^1\text{H NMR}$ ($\text{DMSO } d_6$), δ ppm: 7.04 (d, J = 8.25 Hz, 1H) 7.90 (s, 5H) 8.00 (dd, J = 8.25, 2.02 Hz, 1H) 11.21 (s, 1H)

$^{13}\text{C NMR}$ ($\text{DMSO } d_6$), δ ppm: 109.9, 112.8, 118.5, 118.8, 123.0, 127.0, 132.7, 132.8, 136.8, 143.2, 150.8, 159.5, 184.1.

IR v_{max} (nujol): 3280, 2611, 1822, 1719, 1694, 1627, 1500, 1427 cm^{-1} .

HRMS (ESI) m/z : $\text{C}_{15}\text{H}_8\text{N}_2\text{O}_2$ [$\text{M} + \text{H}$] $^+$, 249.0659; **Found** 249.0660.

5-(2-Cyanophenyl)indoline-2,3-dione (13, BB 0305123) was synthesized according to the **GP2** from **2** (436 mg, 1.00 mmol). Yield: 30%, M = 74 mg. Red solid, m.p. = 206–208 °C.



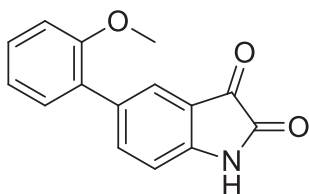
$^1\text{H NMR}$ ($\text{DMSO } d_6$), δ ppm: 7.07 (d, J = 8.19 Hz, 1H), 7.58 (t, J = 7.64 Hz, 1H), 7.63 (d, J = 7.82 Hz, 1H), 7.71 (d, J = 1.59 Hz, 1H), 7.75–7.84 (m, 2H), 7.95 (d, J = 7.70 Hz, 1H), 11.23 (s, 1H).

$^{13}\text{C NMR}$ ($\text{DMSO } d_6$), δ ppm: 110.0, 112.5, 118.2, 118.5, 124.6, 128.3, 129.9, 132.2, 133.6, 133.9, 138.5, 143.1, 150.9, 159.5, 184.0.

IR v_{max} (nujol): 2931, 2920, 2854, 1770, 1734, 1697, 1621, 1608, 1462, 1377, 1302 cm^{-1} .

HRMS (ESI) m/z : $\text{C}_{11}\text{H}_9\text{N}_2\text{O}_2\text{Na}$ [$\text{M} + \text{H}$] $^+$, 249.2363; **Found** 249.2359.

5-(2-Methoxyphenyl)indoline-2,3-dione (14, BB 0223102) was synthesized according to the **GPI** from **1** (273 mg, 1.00 mmol). Yield: 37%, M = 94 mg. Red solid, m.p. = 23 6–238 °C.



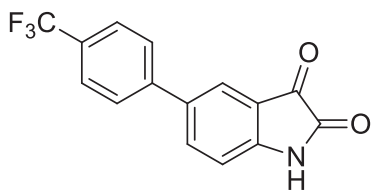
$^1\text{H NMR}$ (DMSO d_6), δ ppm: 3.82 (s, 3H), 6.92 (dd, $J = 8.1, 2.0$ Hz, 1H), 6.99 (d, $J = 8.2$ Hz, 1H), 7.11–7.24 (m, 2H), 7.35 (t, $J = 7.9$ Hz, 1H), 7.77 (d, $J = 1.3$ Hz, 1H), 7.90 (dd, $J = 8.2, 1.6$ Hz, 1H), 11.12 (br. s., 1H).

$^{13}\text{C NMR}$ (DMSO d_6), δ ppm: 55.5, 111.8, 112.0, 117.7, 120.9, 125.1, 128.2, 129.2, 130.0, 132.6, 139.1, 149.5, 156.0, 159.6, 184.5.

IR *vmax* (nujol): 2858, 1952, 1754, 1624, 1604, 1541, 1443, 1377, 1306 cm^{-1} .

HRMS (ESI) *m/z*: $\text{C}_{15}\text{H}_{11}\text{NO}_3$ [$\text{M} + \text{H}$] $^+$, 254.0812; Found 254.0812.

5-(4-(Trifluoromethyl)phenyl)indoline-2,3-dione (15, BB 0223115) was synthesized according to the **GP1** from **1** (273 mg, 1.00 mmol). Yield: 54%, $M = 157$ mg. Red solid, m.p. = 204–206 °C. Spectral data are well consistent with the published ones (Hyun et al., 2010).



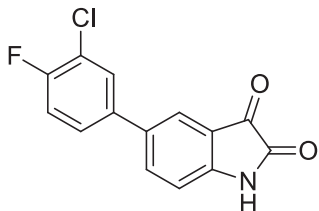
$^1\text{H NMR}$ (DMSO d_6), δ ppm: 7.04 (d, $J = 8.07$ Hz, 1H), 7.79 (d, $J = 8.31$ Hz, 2H), 7.87 (s, 1H), 7.90 (d, 2H, $J = 8.0$ Hz), 7.98 (dd, $J = 8.25, 1.90$ Hz, 1H), 11.20 (s, 1H).

$^{13}\text{C NMR}$ (DMSO d_6), δ ppm: 112.8, 118.6, 122.9, 125.8 (q, $J = 3.7$ Hz), 125.8, 127.0, 127.8 (q, $J = 32.9$ Hz), 133.1, 136.8, 142.7, 150.7, 159.5, 184.2.

IR *vmax* (nujol): 3364, 2872, 1841, 1740, 1688, 1603, 1540, 1488, 1379 cm^{-1} .

HRMS (ESI) *m/z*: $\text{C}_{15}\text{H}_8\text{F}_3\text{NO}_2$ [$\text{M} + \text{H}$] $^+$, 292.0604; Found 292.0607.

5-(3-Chloro-4-fluorophenyl)indoline-2,3-dione (16, BB 0305130) was synthesized according to the **GP2** from **2** (436 mg, 1.00 mmol). Yield: 28%, $M = 77$ mg. Red solid, m.p. = 244–246 °C



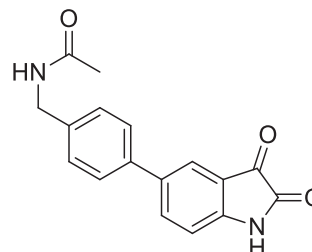
$^1\text{H NMR}$ (DMSO d_6), δ ppm: 7.00 (d, $J = 8.07$ Hz, 1H), 7.31 (td, $J = 8.28, 2.26$ Hz, 1H), 7.48 (dd, $J = 8.13, 6.79$ Hz, 1H), 7.52 (s, 1H), 7.57 (dd, $J = 8.93, 2.45$ Hz, 1H), 7.63 (d, $J = 8.19$ Hz, 1H), 11.17 (s, 1H).

$^{13}\text{C NMR}$ (DMSO d_6), δ ppm: 112.6, 117.2 (d, $J = 21.2$ Hz), 118.4, 120.1 (d, $J = 18.3$ Hz), 122.8, 126.9 (d, $J = 6.6$ Hz), 128.3, 132.5, 136.5, 150.3, 156.8 (d, $J = 248.1$ Hz), 159.5, 184.2.

IR *vmax* (nujol): 3421(br), 3163(br), 2929, 2918, 2854, 1751, 1624, 1462, 1377, 1261 cm^{-1} .

HRMS (ESI) *m/z*: $\text{C}_{14}\text{H}_8\text{ClFNO}_2$ [$\text{M} + \text{H}$] $^+$, 276.0222; Found 276.0222.

N-(4-(2,3-Dioxindolin-5-yl)benzyl)acetamide (17, BB 0305118) was synthesized according to the **GP2** from **2** (436 mg, 1.00 mmol). Yield: 12%, $M = 35$ mg. Red solid, m.p. = 226–228 °C.



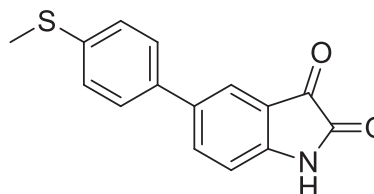
$^1\text{H NMR}$ (DMSO d_6), δ ppm: 1.88 (s, 3H), 4.27 (d, $J = 5.99$ Hz, 2H), 7.00 (d, $J = 8.19$ Hz, 1H), 7.32 (d, $J = 8.19$ Hz, 2H), 7.61 (d, $J = 8.31$ Hz, 2H), 7.75 (d, $J = 1.71$ Hz, 1H), 7.89 (dd, $J = 8.19, 1.96$ Hz, 1H), 8.36 (t, $J = 5.81$ Hz, 1H), 11.11 (s, 1H).

$^{13}\text{C NMR}$ (DMSO d_6), δ ppm: 22.6, 41.8, 112.6, 118.4, 122.3, 126.1, 127.9, 134.7, 136.3, 137.2, 139.0, 149.8, 159.5, 169.1, 184.4.

IR *vmax* (nujol): 2858, 1952, 1754, 1624, 1604, 1541, 1443, 1377, 1306 cm^{-1} .

HRMS (ESI) *m/z*: $\text{C}_{17}\text{H}_{15}\text{N}_2\text{O}_3$ [$\text{M} + \text{H}$] $^+$, 295.1077; Found 295.1077.

5-(4-(Methylthio)phenyl)indole-2,3-dione (18, BB 0223099) was synthesized according to the **GP1** from **1** (273 mg, 1.00 mmol). Yield: 32%, $M = 83$ mg. Red solid, m.p. = 212–214 °C.



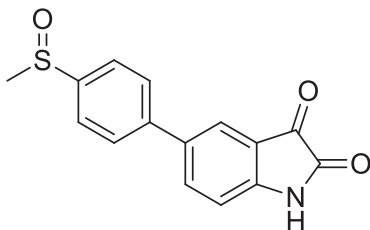
$^1\text{H NMR}$ (DMSO d_6), δ ppm: 3.40 (s, 3H), 6.98 (d, $J = 8.1$ Hz, 1H), 7.31 (d, $J = 8.2$ Hz, 2H), 7.58 (d, $J = 8.2$ Hz, 2H), 7.73 (s, 1H), 7.86 (d, $J = 7.9$ Hz, 1H), 11.14 (s, 1H).

$^{13}\text{C NMR}$ (DMSO d_6), δ ppm: 14.6, 112.7, 118.4, 122.1, 126.3, 126.6, 134.3, 135.2, 136.1, 137.6, 149.8, 159.6, 184.4.

IR *vmax* (nujol): 2841, 1817, 1659, 1601, 1543, 1420, 1360, 1300 cm^{-1} .

HRMS (ESI) m/z : $C_{15}H_{11}NO_2S$ $[M+H]^+$, 270.0583; **Found** 270.0582

5-(4-(Methylsulphenyl)phenyl)indole-2,3-dione (19, BB 0300735)



Compound **18** (538 mg, 2.00 mmol, 1 equiv) was dissolved in AcOH (7.4 mL), then hydrogen peroxide (0.084 mL, 2.00 mmol, 1 equiv) was slowly added by dropwise. The mixture was reflux for 5 min and cooled to r.t. The resulting solution was extracted with Et₂O, dried over anhydrous MgSO₄, filtered and evaporated under reduced pressure. Yield 18%, M = 103 mg. Red solid. m.p. = 218–220 °C

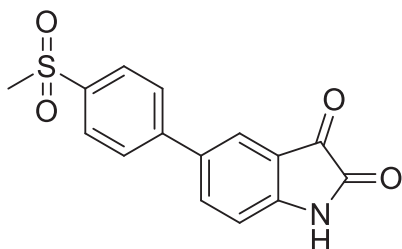
¹H NMR (DMSO d_6), δ ppm: 2.78 (s, 3H), 7.02 (d, J = 8.2 Hz, 1H), 7.74 (d, J = 8.4 Hz, 2H), 7.82–7.90 (m, 3H), 7.96 (dd, J = 8.3, 1.9 Hz, 1H), 11.18 (s, 1H).

¹³C NMR (DMSO d_6), δ ppm: 21.1, 43.2, 112.8, 118.6, 122.8, 124.4, 127.1, 133.6, 136.7, 141.0, 145.3, 150.4, 159.6, 172.1, 184.3.

IR ν_{max} (nujol): 3421(br), 2929, 2918, 2854, 1624, 1462, 1377, 1261 cm^{-1} .

HRMS (ESI) m/z : $C_{15}H_{11}NO_3S$ $[M+H]^+$, 286.0532; **Found** 286.0530.

5-(4-(Methylsulfonyl)phenyl)indoline-2,3-dione (20, BB 0223960) was synthesized according to the **GPI** from **1** (273 mg, 1.00 mmol). Yield: 37%, M = 111 mg. Red solid, m.p. = 258–260 °C



¹H NMR (DMSO d_6), δ ppm: 3.25 (s, 3H), 7.04 (d, J = 8.19 Hz, 1H), 7.88 (s, 1H), 7.91–8.01 (m, 5H), 11.21 (s, 1H).

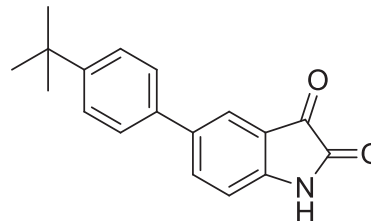
¹³C NMR (DMSO d_6), δ ppm: 43.5, 112.8, 118.6, 123.1, 127.0, 127.7, 132.9, 136.9, 139.5, 143.60, 150.8, 159.5, 184.1.

IR ν_{max} (nujol): 3418, 2872, 2850, 1772, 1730, 1518, 1400, 1382, 1225 cm^{-1} .

HRMS (ESI) m/z : $C_{15}H_{11}NO_4S$ $[M+H]^+$, 301.3171; **Found** 301.3170.

5-(4-(*tert*-Butyl)phenyl)indoline-2,3-dione (21, BB 0223799) was synthesized according to the **GPI** from **1** (273 mg,

1.00 mmol). Yield: 55%, M = 153 mg. Red solid, m.p. = 182–184 °C. Spectral data are well consistent with the published ones ([Zhang et al., 2018](#)).



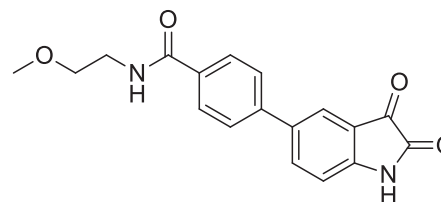
¹H NMR (DMSO d_6), δ ppm: 1.30 (s, 9H), 6.99 (d, J = 8.07 Hz, 1H), 7.46 (d, J = 8.07 Hz, 2H), 7.57 (d, J = 8.31 Hz, 2H), 7.73 (s, 1H), 7.87 (d, J = 8.19 Hz, 1H), 11.12 (s, 1H).

¹³C NMR (DMSO d_6), δ ppm: 31.1, 34.3, 112.7, 118.4, 122.2, 125.8, 125.9, 134.8, 135.9, 136.3, 138.4, 149.8, 149.9, 159.6, 184.4.

IR ν_{max} (nujol): 3394, 2924, 2858, 1752, 1739, 1624, 1603, 1541, 1464, 1377, 1306 cm^{-1} .

HRMS (ESI) m/z : $C_{18}H_{17}NO_2$ $[M+H]^+$, 280.3331; **Found** 280.3333.

4-(2,3-Dioxindolin-5-yl)-N-(2-methoxyethyl)benzamide (22, BB 0300746) was synthesized according to the **GPI** from **1** (273 mg, 1.00 mmol). Yield: less than 5%, M = 32 mg. Red solid, m.p. = 212–213 °C



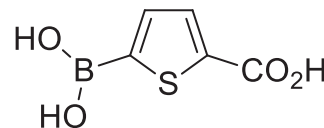
¹H NMR (DMSO d_6), δ ppm: 3.27 (s, 3H), 3.36–3.50 (m, 4H), 7.02 (d, J = 8.0 Hz, 1H), 7.76 (d, J = 8.4 Hz, 2H), 7.85 (d, J = 1.8 Hz, 1H), 7.92 (d, J = 8.4 Hz, 2H), 7.97 (dd, J = 8.4, 2.0 Hz, 1H), 8.55 (br. s., 1H)

¹³C NMR (DMSO d_6), δ ppm: (ppm) 54.2, 57.9, 70.4, 112.7, 118.5, 122.6, 125.9, 127.9, 133.1, 133.8, 136.5, 141.1, 150.3, 157.6, 159.5, 184.2.

IR ν_{max} (nujol): 3394, 2924, 2858, 1752, 1739, 1624, 1603, 1541, 1464, 1377, 1306 cm^{-1} .

HRMS (ESI) m/z : $C_{18}H_{17}N_2O_4$ $[M+H]^+$, 324.3306; **Found** 324.3302.

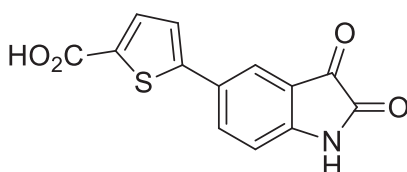
5-Boronothiophene-2-carboxylic acid (24, CAS 465515–31–5)



Thiophene-2-carboxylic acid (**23**) (3.84 g, 30.0 mmol, 1 equiv) was dissolved in THF (0.1 M). After solution forming, reaction mixture was cooled to $-78\text{ }^{\circ}\text{C}$ and lithium diisopropyl amide (60.0 mmol, 2 equiv) was added dropwise. Then, triisopropyl borate (6.92 mL, 30.0 mmol, 1 equiv) was added into this reaction mixture at $-78\text{ }^{\circ}\text{C}$. Then reaction mixture was warmed to r.t. and poured into saturated ammonia hydrochloride. Mixture was extracted with ethyl acetate ($3 \times 100\text{ mL}$) and evaporated by rotary evaporation with low pressure.

$^1\text{H NMR}$ (DMSO d_6), δ ppm: 7.50–7.70 (br. s, 2H), 7.67 (d, $J = 3.6\text{ Hz}$, 1H), 7.30 (d, $J = 3.6\text{ Hz}$, 1H), 7.79 (d, $J = 3.6\text{ Hz}$, 1H). Spectral data are well consistent with the published ones (Witschel Matthias et al., 2015).

5-(2,3-Dioxindolin-5-yl)thiophene-2-carboxylic acid (**25**, BB 0323214) was synthesized according to the **GPI** from **1** (273 mg, 1.00 mmol). Yield: 91%, $M = 248\text{ mg}$. Red solid, m.p. = $325\text{--}327\text{ }^{\circ}\text{C}$.



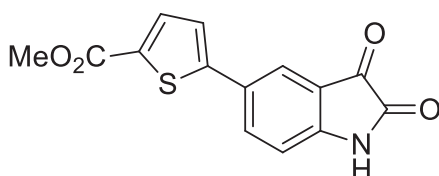
$^1\text{H NMR}$ (DMSO d_6), δ ppm: 7.00 (d, $J = 8.2\text{ Hz}$, 1H), 7.16 (d, $J = 3.6\text{ Hz}$, 1H), 7.30 (d, $J = 3.6\text{ Hz}$, 1H), 7.66 (d, $J = 1.8\text{ Hz}$, 1H), 7.80 (dd, 1H).

$^{13}\text{C NMR}$ (DMSO d_6), δ ppm: 113.1, 118.4, 120.6, 123.1, 128.1, 129.3, 134.8, 142.5, 147.7, 150.4, 159.8, 164.1, 173.2, 184.8.

IR ν_{max} (nujol): 3671, 2740, 1811, 1690, 1600, 1430, 1355, 1290, 812 cm^{-1} .

HRMS (ESI) m/z : $\text{C}_{14}\text{H}_9\text{NO}_4\text{S}$ $[\text{M} + \text{Na}]^+$, 296.2532; Found 296.2535.

Methyl 5-(2,3-dioxindolin-5-yl)thiophene-2-carboxylate (**26**, BB 0300739)



Acid **25** (273 mg, 1.00 mmol, 1 equiv) was dissolved in saturated by HCl methanol (1 M) and stirred and reflux for a 5 h. Then, after cooling to a r.t mixture was evaporated under reduced pressure. Yield 85%, $M = 244\text{ mg}$. Red solid, m.p. = $254\text{--}256\text{ }^{\circ}\text{C}$

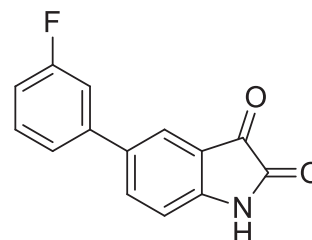
$^1\text{H NMR}$ (DMSO d_6), δ ppm: 3.83 (s, 3H), 6.99 (d, $J = 8.19\text{ Hz}$, 1H), 7.62 (d, $J = 3.67\text{ Hz}$, 1H), 7.78 (d, $J = 3.67\text{ Hz}$, 1H), 7.86 (s, 1H), 7.94 (d, $J = 7.21\text{ Hz}$, 1H), 11.22 (br. s., 1H).

$^{13}\text{C NMR}$ (DMSO d_6), δ ppm: 48.6, 52.3, 112.89, 118.6, 121.7, 124.5, 127.4, 130.8, 134.9, 135.5, 149.1, 150.8, 159.4, 161.7, 183.8.

IR ν_{max} (nujol): 3623, 2922, 2854, 1745, 1711, 1622, 1460, 1377, 1315, 756 cm^{-1} .

HRMS (ESI) m/z : $\text{C}_{14}\text{H}_9\text{NO}_4\text{S}$ $[\text{M} + \text{Na}]^+$, 310.2798; Found 310.2799.

5-(3-Fluorophenyl)indoline-2,3-dione (**27**, BB 0223094) was synthesized according to the **GPI** from **1** (273 mg, 1.00 mmol). Yield: 45%, $M = 109\text{ mg}$. Red solid, m.p. = $212\text{--}214\text{ }^{\circ}\text{C}$.



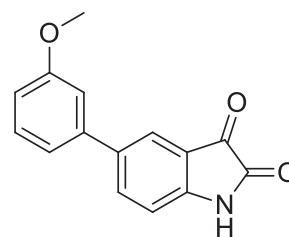
$^1\text{H NMR}$ (DMSO d_6), δ ppm: 6.97 (d, $J = 8.2\text{ Hz}$, 1H), 7.10–7.20 (m, 1H), 7.38–7.54 (m, 3H), 7.79 (d, $J = 1.7\text{ Hz}$, 1H), 7.91 (dd, $J = 8.2, 2.0\text{ Hz}$, 1H), 11.17 (s, 1H).

$^{13}\text{C NMR}$ (DMSO d_6), δ ppm: 112.7, 113.0 (d, $J = 22.6\text{ Hz}$), 114.2 (d, $J = 21.1\text{ Hz}$), 118.4, 122.3, 122.7, 130.9 (d, $J = 8.7\text{ Hz}$), 133.4, 136.6, 141.1 (d, $J = 7.8\text{ Hz}$), 150.4, 159.6, 162.7 (d, $J = 243.1\text{ Hz}$), 184.2.

IR ν_{max} (nujol): 3623, 2922, 2854, 1745, 1711, 1622, 1460, 1377, 1315, 756 cm^{-1} .

HRMS (ESI) m/z : $\text{C}_4\text{H}_8\text{FNO}_2$ $[\text{M} + \text{H}]^+$, 242.0612; Found 242.0612.

5-(3-Methoxyphenyl)indoline-2,3-dione (**28**, BB 0223101) was synthesized according to the **GPI** from **1** (273 mg, 1.00 mmol). Yield: 48%, $M = 121\text{ mg}$. Red solid, m.p. $210\text{--}212\text{ }^{\circ}\text{C}$. Spectral data are well consistent with the published ones (Babu et al., 2018).



$^1\text{H NMR}$ (DMSO d_6), δ ppm: 3.76 (s, 3H), 6.95 (d, $J = 8.2\text{ Hz}$, 1H), 7.01 (t, $J = 7.5\text{ Hz}$, 1H), 7.10 (d, $J = 8.2\text{ Hz}$, 1H), 7.27 (dd, $J = 7.5, 1.5\text{ Hz}$, 1H), 7.33 (dd, $J = 15.6, 1.5\text{ Hz}$, 1H), 7.56 (d, $J = 1.5\text{ Hz}$, 1H), 7.67 (dd, $J = 8.2, 1.7\text{ Hz}$, 1H), 11.10 (s, 1H).

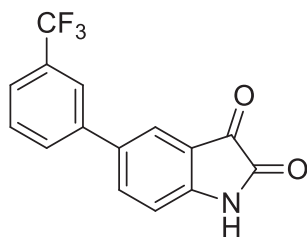
$^{13}\text{C NMR}$ (DMSO d_6), δ ppm: 55.8, 112.6, 121.1, 123.5, 126.9, 130.2, 133.4, 138.8, 147.3, 149.4, 154.9, 156.9, 158.9, 180.6, 185.3.

IR ν_{max} (nujol): 3623, 2922, 2854, 1745, 1711, 1622, 1460, 1377, 1315, 756 cm^{-1} .

HRMS (ESI) m/z : $\text{C}_{15}\text{H}_{11}\text{NO}_3$ $[\text{M} + \text{Na}]^+$, 276.0631; Found 276.0632

5-(3-(Trifluoromethyl)phenyl)indoline-2,3-dione (**29**, BB 0223116) was synthesized according to the **GPI** from **1**

(273 mg, 1.00 mmol). Yield: 42%, M = 122 mg. Red solid, m.p. = 246–248 °C.



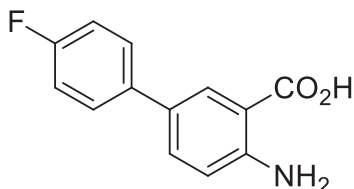
¹H NMR (DMSO *d*₆), δ ppm: 7.03 (d, *J* = 8.19 Hz, 1H), 7.64–7.74 (m, 2H), 7.91 (d, *J* = 1.90 Hz, 1H), 7.95–8.03 (m, 3H), 11.18 (s, 1H).

¹³C NMR (DMSO *d*₆), δ ppm: 112.7, 118.5, 122.8 (q, *J* = 3.7 Hz), 124.0 (q, *J* = 3.7 Hz), 125.6, 129.7, 130.0, 130.1, 131.8 (q, *J* = 285.4 Hz) 136.8, 139.8, 150.5, 159.5, 184.2.

IR *ν*_{max} (nujol): 3421(br.), 3163(br.), 2929, 2918, 2854, 1751, 1624, 1462, 1377, 1261 cm⁻¹.

HRMS (ESI) *m/z*: C₁₅H₈F₃NO₂ [M+Na]⁺, 314.0424; Found 314.0416.

4-Amino-4'-fluoro-[1,1'-biphenyl]-3-carboxylic acid (30, BB 0223070)



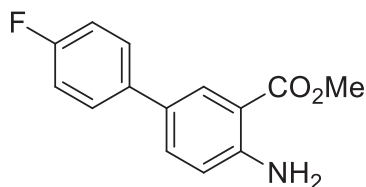
5-(4-(Fluoro)phenyl)indoline-2,3-dione (7) (996 mg, 4.00 mmol, 1 equiv) was dissolved in 20% NaOH (672 mg, 12.00 mmol, 3 equiv). Hydrogen peroxide (0.56 mL, 8.00 mmol, 2 eq) was added dropwise and the reaction mixture stirred for 4 h, then poured into water and filtered off. Solid was washed by DCM, and diethyl ester and dried under high vacuum. Yield: 32%, M = 300 mg. Grey solid, m.p = 154–156 °C.

¹H NMR (DMSO *d*₆), δ ppm: 6.80 (d, *J* = 8.56 Hz, 1H), 7.20 (t, *J* = 8.74 Hz, 2H), 7.49 (d, *J* = 9.90 Hz, 1H), 7.56 (dd, *J* = 8.13, 5.56 Hz, 2H), 7.99 (d, 1H).

¹³C NMR (DMSO *d*₆), δ ppm: 112.4, 115.5, 115.7, 116.9, 125.3, 127.2, 127.3, 129.1, 131.2, 136.7, 136.7, 150.7, 159.8, 162.2, 170.3, 172.3.

HRMS (ESI) *m/z*: C₁₄H₁₄NO₂ [M+H]⁺, 214.0863; Found 214.0861

Methyl 4-amino-4'-fluoro-[1,1'-biphenyl]-3-carboxylate (31, BB 0305126)



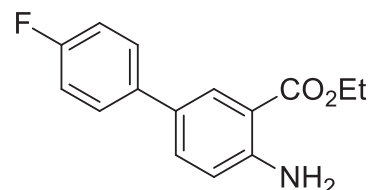
Acid **30** (227 mg, 1.00 mmol, 1 equiv), was dissolved in MeOH (10 mL), then sulfuric acid (2.54 mL, 10.00 mmol, 10 equiv) was added dropwise with cooling at the ice bath. The reaction was stirred for 5 h, then poured into ice and potassium carbonate was added to neutral pH, then mixture was extracted with ethyl acetate (3x 100 mL). The organic layer was dried over sodium sulfate, filtered off and filtrate was evaporated under reduced pressure. Yield: 87%. M = 213 mg. Grey solid, m.p = 90–93 °C. Spectral data are well consistent with the published ones (Nakamura et al., 2017).

¹H NMR (DMSO), δ ppm: 3.82 (s, 3H), 6.77 (s, 2H), 6.88 (d, *J* = 8.7 Hz, 1H), 7.21 (t, *J* = 8.8 Hz, 2H), 7.48–7.63 (m, 3H), 7.94 (d, 1H)

¹³C NMR (DMSO), δ ppm: 20.6, 51.5, 108.9, 117.3, 125.3, 126.7, 127.9, 129.5, 132.3, 135.4, 136.8, 150.6, 167.8.

HRMS (ESI) *m/z*: C₁₅H₁₆NO₄ [M+H]⁺, 241.2851; Found 241.2852.

Ethyl 4-amino-4'-fluoro-[1,1'-biphenyl]-3-carboxylate (32, BB 0305127)



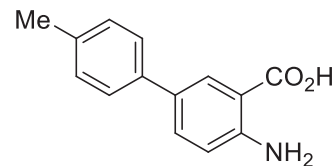
Acid **30** (227 mg, 1.00 mmol, 1 equiv), was dissolved in ethanol (10 mL, 0.1 M), then sulfuric acid (2.54 mL, 10.00 mmol, 10 equiv) was added slowly by dropwise. The reaction mixture was stirred for 5 h, then poured into ice and potassium carbonate was added to neutral pH and mixture was extracted with ethyl acetate (3x 100 mL). The organic layer was dried over sodium sulfate, filtered off and evaporated under reduced pressure. Yield: 64%, M = 166 mg. Grey solid, m.p = 138–140 °C

¹H NMR (CDCl₃), δ ppm: 1.42 (t, *J* = 7.09 Hz, 3H), 4.38 (q, *J* = 7.09 Hz, 2H), 6.76 (d, *J* = 8.56 Hz, 1H), 7.11 (t, *J* = 8.62 Hz, 2H), 7.43–7.58 (m, 3H), 8.07 (d, 1H).

¹³C NMR (CDCl₃), δ ppm: 14.3, 60.4, 111.1, 115.3, 115.5, 117.2, 127.6, 127.7, 128.3, 129.2, 132.5, 136.5, 136.6, 149.6, 160.6, 163.0, 168.0.

HRMS (ESI) *m/z*: C₁₅H₁₆NO₄ [M+H]⁺, 241.2851; Found 241.2852.

4-Amino-4'-methyl-[1,1'-biphenyl]-3-carboxylic acid (BB 0223071)



5-(4-(Methyl)phenyl)indoline-2,3-dione was synthesized according to the literature procedure (Agamennone et al., 2016) from 5-bromisatin (2.26 g, 10.0 mmol). 5-(4-(Methyl)phe

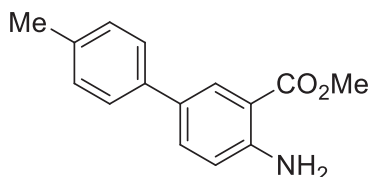
nyl)indoline-2,3-dione (1 g, 4.00 mmol, 1 equiv) was dissolved in 20% NaOH (896 mg, 12.00 mmol, 4 equiv). Then hydrogen peroxide (0.6 mL, 8.00 mmol, 2 equiv) was added slowly by dropwise. The result mixture was stirred for 4 h, then poured into ice and filtered off. Solid was washed by DCM and diethyl ester, and dried under high vacuum. Yield: 49%, M = 450 mg. Grey solid, m.p = 150–152 °C

$^1\text{H NMR}$ (DMSO d_6), δ ppm: 6.80 (d, J = 8.56 Hz, 1H), 7.20 (t, J = 8.74 Hz, 2H), 7.49 (d, J = 9.90 Hz, 1H), 7.56 (dd, J = 8.13, 5.56 Hz, 2H), 7.99 (d, 1H).

$^{13}\text{C NMR}$ (DMSO d_6), δ ppm: 20.6, 40.1, 116.9, 125.2, 126.3, 128.7, 129.4, 131.2, 135.1, 137.2, 150.6, 160.9, 170.0.

HRMS (ESI) m/z : $\text{C}_{14}\text{H}_{14}\text{NO}_2$ [$\text{M} + \text{H}$] $^+$, 214.0863; Found 214.0861.

Methyl 4-amino-4'-methyl-[1,1'-biphenyl]-3-carboxylate (33, BB 0304409)



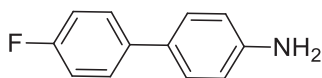
BB 0,223,071 (227.0 mg, 1.00 mmol, 1 equiv), was dissolved in methanol (10 mL), then sulfuric acid (2.54 mL, 10.00 mmol, 10 equiv) was added slowly by dropwise. The reaction mixture was stirred for 5 h, then poured into ice and potassium carbonate was added to neutral pH and mixture was extracted with ethyl acetate (3x 100 mL). The organic layer was dried over sodium sulfate, filtered off and evaporated under reduced pressure. Yield: 91%, M = 212 mg. Grey solid, m.p = 152 °C

$^1\text{H NMR}$ (CDCl_3), δ ppm: 2.31 (s, 3H), 3.82 (s, 3H), 6.74 (s, 2H), 6.87 (d, J = 8.6 Hz, 1H), 7.21 (d, J = 7.9 Hz, 2H), 7.43 (d, J = 7.9 Hz, 2H), 7.58 (dd, J = 8.6, 2.2 Hz, 1H), 7.95 (d, 1H).

$^{13}\text{C NMR}$ (CDCl_3), δ ppm: 20.6, 51.5, 108.9, 117.3, 125.3, 126.7, 127.9, 129.5, 132.3, 135.4, 136.8, 150.6, 167.8.

HRMS (ESI) m/z : $\text{C}_{15}\text{H}_{16}\text{NO}_4$ [$\text{M} + \text{H}$] $^+$, 241.2851; Found 241.2852.

4'-Fluoro-[1,1'-biphenyl]-4-amine (34, BB 0222486)

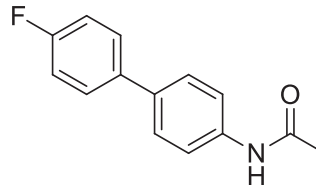


4-Fluoro phenyl boronic acid (2.78 g, 20.00 mmol, 1 equiv), was dissolved in a mixture of solvents ethanol : water (1:1, 50 mL), then 4-bromoaniline (3.91 mL, 20.00 mmol, 1 equiv), potassium carbonate (8.28 g, 60.00 mmol, 3 equiv), triphenylphosphine (262 mg, 1.00 mmol) and Pd(dba) $_2$ (575 mg, 0.5 mmol) were added. The reaction mixture was heated to reflux for 6 h, then cooled to r.t and filtered off. The crude material was washed with ether and dried under high vacuum. Yield: 64%, M = 2.4 g. White solid, m.p = 98–100 °C. Spectral data are well consistent with the published ones (Huifeng et al., 2017).

$^1\text{H NMR}$ (DMSO d_6), δ ppm: 6.62 (d, 2H), 7.16 (t, J = 8.9 Hz, 2H), 7.30 (d, J = 8.4 Hz, 2H), 7.53 (dd, J = 8.7, 5.5 Hz, 2H).

$^{13}\text{C NMR}$ (DMSO d_6), δ ppm: 114.2, 115.3, 115.5, 126.5, 127.1, 127.2, 137.3, 137.3, 148.3, 159.6, 162.0.

N-(4'-Fluoro-[1,1'-biphenyl]-4-yl)acetamide (35, BB 0305129)



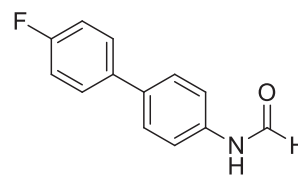
Aniline **34** (935 mg, 5.00 mmol, 1 equiv), was dissolved in DCM (50 mL, 0.1 M), then trimethylamine (0.695 mL, 5.00 mmol, 1 equiv) was added. After 5 min stirring, AcCl (0.39 mL, 5.00 mmol, 1 equiv) was added dropwise and the reaction was stirred for another 2 h, then mixture was poured into water and extracted it off. The organic layer was dried over sodium sulfate, filtered and evaporated under reduced pressure. Yield: 95%, M = 1.09 g. Brown solid, m.p = 198–200 °C. Spectral data are well consistent with the published ones (Schmidt et al., 2015).

$^1\text{H NMR}$ (DMSO d_6), δ ppm: 2.06 (br. s., 3H), 7.25 (t, J = 8.31 Hz, 2H), 7.51–7.76 (m, 6H), 10.04 (br. s., 1H).

$^{13}\text{C NMR}$ (DMSO d_6), δ ppm: 24.1, 115.5, 115.8, 119.3, 126.9, 128.10, 128.2, 133.6, 136.3, 138.8, 160.4, 162.8, 168.4.

HRMS (ESI) m/z : $\text{C}_{14}\text{H}_{13}\text{FNO}$ [$\text{M} + \text{H}$] $^+$, 229.2496; Found 229.2496.

N-(4'-Fluoro-[1,1'-biphenyl]-4-yl)formamide (36, BB 0305128)



Aniline **34** (935 mg, 5.00 mmol, 1 equiv), was dissolved in toluene (50 mL, 0.1 M), then formic acid (4.3 mL, 20.00 mmol, 4 equiv) was added. The reaction mixture was stirred and reflux for 2 h then poured into saturated sodium hydrocarbonate and extracted with ethyl acetate. The organic layer was dried over sodium sulfate, filtered and evaporated under reduced pressure. Yield: 92%, M = 989 mg. Brown solid, m.p = 109–110 °C

$^1\text{H NMR}$ (DMSO d_6), δ ppm: 7.25 (t, J = 8.8 Hz, 2H), 7.49–7.74 (m, 6H), 8.30 (s, 1H), 10.27 (br. s., 1H)

$^{13}\text{C NMR}$ (DMSO d_6), δ ppm: 115.5, 115.7, 117.8, 119.5, 127.0, 127.5, 128.1, 128.2, 134.3, 136.1, 137.6, 159.6, 160.4, 162.4, 162.8.

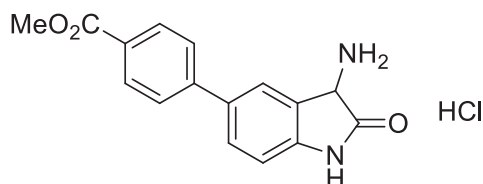
HRMS (ESI) m/z : $\text{C}_{14}\text{H}_{13}\text{FNO}$ [$\text{M} + \text{H}$] $^+$, 216.2230; Found 216.2235.

Compounds **37–39** and **42**, where obtained via oxime formation from the corresponding isatin-based derivative^{S11}. Compounds **40** and **41** have been respectively prepared from the acetylation and mesilation of 3-amino-5-(p-tolyl)indolin-2-one (Agamennone et al., 2016).

4.2.4. General procedure (GP3) for the synthesis of 5-Aryl-3-aminoindole-2-ones

Oxime (1 equiv) was dissolved in methanol (0.5 M), then AcOH (1 equiv) was added. When clear solution is forming, 10% Pd/C (10% mass) was added. Reaction mixture was degased and setup in hydrogen atmosphere Mixture was stirred for a 8 h, then filtered off through cellite and solid was washed with boiled methanol. Filtrate was evaporated under reduced pressure and crude material was titrated with diethyl ester and filtered off.

Methyl 4-(3-Amino-2-oxoindolin-5-yl)benzoate hydrochloride (37, BB 0270669) was synthesized according to the GP3 from **37b** (296 mg, 1.00 mmol). Yield: 85%, M = 273 mg. White solid, m.p. = 287–289 °C



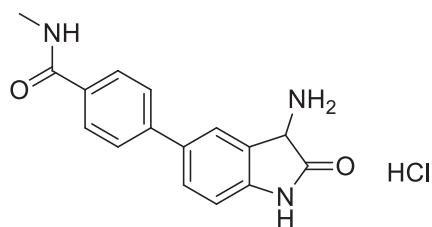
¹H NMR (DMSO *d*₆), δ ppm: 3.87 (s, 3H), 5.03 (s, 1H), 7.04 (d, *J* = 8.19 Hz, 1H), 7.76 (d, *J* = 8.44 Hz, 3H), 8.04 (d, *J* = 8.31 Hz, 2H), 8.24 (s, 1H), 9.27 (br. s., 3H), 11.13 (s, 1H).

¹³C NMR (DMSO *d*₆), δ ppm: 50.7, 52.1, 110.6, 124.4, 124.8, 126.1, 128.0, 128.9, 129.9, 132.5, 143.4, 144.3, 166.0, 173.1.

IR *v*_{max} (nujol): 3511, 3302, 2987, 2932, 2810, 1935, 1717, 1525, 1367, 1303, 1110 cm⁻¹.

HRMS (ESI) *m/z*: C₁₆H₁₄N₂O₃ [M+H]⁺, 283.1077; Found 283.1072.

4-(3-Amino-2-oxoindolin-5-yl)-N-methylbenzamide hydrochloride (38, BB 0300738) was synthesized according to the GP3 from **38b** (295 mg, 1.00 mmol). Yield: 90%, M = 285 mg.



White solid m.p. = 300–302 °C

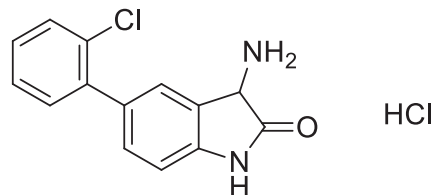
¹H NMR (DMSO *d*₆), δ ppm: 2.80 (s, 3H), 3.16 (s, 1H), 5.03 (br. s., 1H), 7.02 (d, *J* = 8.07 Hz, 1H), 7.53–7.81 (m, 3H), 7.94 (d, *J* = 8.19 Hz, 2H), 8.20 (s, 1H), 8.52 (d, *J* = 4.52 Hz, 1H), 9.24 (br. s., 3H), 11.07 (s, 1H).

¹³C NMR (DMSO *d*₆), δ ppm: 26.2, 50.8, 110.6, 124.2, 124.6, 125.7, 127.9, 128.7, 132.9, 133.0, 142.1, 142.9, 166.2, 173.1.

IR *v*_{max} (nujol): 3394, 2924, 2858, 1752, 1739, 1624, 1603, 1541, 1464, 1377, 1306 cm⁻¹

HRMS (ESI) *m/z*: C₁₆H₁₅N₃O₂ [M+H]⁺, 282.1237; Found 282.1232.

3-Amino-5-(2-chlorophenyl)indole-2-one hydrochloride (39, BB 0300736) was synthesized according to the GP3 from **39b** (272 mg, 1.00 mmol). Yield: 83%, M = 245 mg. White solid m.p. = 286–288 °C



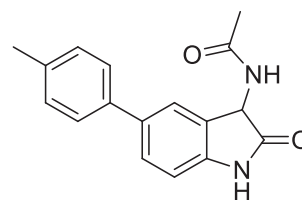
¹H NMR (DMSO *d*₆), δ ppm: 5.01 (s, 1H), 7.02 (d, *J* = 7.9 Hz, 1H), 7.31–7.46 (m, 5H), 7.57 (dd, *J* = 7.7, 1.3 Hz, 1H), 7.86 (s, 1H), 9.24 (br. s., 3H), 11.09 (s, 1H).

¹³C NMR (DMSO *d*₆), δ ppm: 50.7, 109.9, 123.4, 127.0, 127.6, 129.1, 130.0, 131.3, 131.3, 131.4, 132.4, 139.4, 142.7, 173.1.

IR *v*_{max} (nujol): 3237, 1769, 1738, 1728, 1716, 1620, 1465, 1456, 1201, 836, 741 cm⁻¹.

HRMS (ESI) *m/z*: C₁₄H₁₂ClN₂O [M+H]⁺, 259.0633; Found 259.0626.

N-[2-Oxo-5-(p-tolyl)indolin-3-yl]acetamide (40, BB 0300740)



Compound **40** was prepared by a direct acylation on the 3-amino-5-(p-tolyl)indolin-2-one substrate, which preparation and characterization is described in a previous work (Agamennone et al., 2016).

3-Amino-5-(p-tolyl)indolin-2-one (238 mg, 1.00 mmol, 1 equiv) was dissolved in DCM (1 M), then trimethylamine (0.139 mL, 1.00 mmol, 1 equiv) was added. Then into reaction mixture AcCl (0.067 mL, 1.00 mmol, 1 equiv) was added dropwise. Reaction mixture was stirred for 5 h, then poured into water and extracted with DCM. Organic layer was dried over sodium sulfate and filtered off. Filtrate was evaporated under reduced pressure. Yield 90%, M = 173 mg. White solid m.p. = 286–288 °C

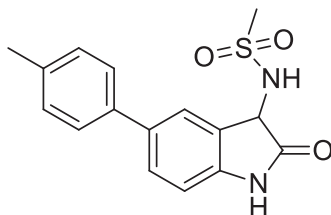
¹H NMR (DMSO *d*₆), δ ppm: 1.89 (s, 3H), 2.30 (s, 3H), 5.12 (d, *J* = 7.9 Hz, 1H), 6.86 (d, *J* = 8.0 Hz, 1H), 7.21 (d, *J* = 7.8 Hz, 2H), 7.34 (s, 1H), 7.45 (d, *J* = 7.8 Hz, 3H), 8.70 (d, *J* = 8.0 Hz, 1H), 10.50 (br. s., 1H)

¹³C NMR (DMSO *d*₆), δ ppm: 20.7, 22.3, 52.4, 109.8, 121.8, 126.1 (2C), 126.7, 128.9, 129.6 (2C), 133.8, 136.1, 137.4, 141.8, 169.5, 175.8

IR *v*_{max} (nujol): 3367, 1810, 11730, 1725, 1515, 1443, 1416, 1199, 842 cm⁻¹.

HRMS (ESI) m/z : $C_{14}H_{12}ClN_2O$ $[M+H]^+$, 280.3211; **Found** 280.3212.

N-[2-Oxo-5-(p-tolyl)indolin-3-yl]methanesulfonamide (41, BB 0300744)



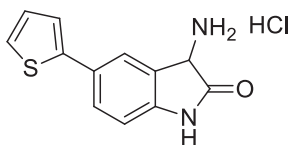
Compound **41** was prepared by a direct mesylation on the 3-amino-5-(p-tolyl)indolin-2-one substrate, which preparation and characterization is described in a previous work^{S11}. 3-Amino-5-(p-tolyl)indolin-2-one (238 mg, 1.00 mmol, 1 eq) was dissolved in DCM (1 M), then trimethylamine (0.139 mL, 1.00 mmol, 1 eq) was added. Then into reaction mixture MsCl (0.079 mL, 1.00 mmol, 1 eq) was added dropwise. Reaction mixture was stirred for 5 h, then poured into water and extracted with DCM. Organic layer was dried over sodium sulfate and filtered off. Filtrate was evaporated under reduced pressure. Yield 90%, M = 163 mg. White solid m.p. = 244–246 °C

1H NMR (DMSO d_6), δ ppm: 2.32 (s, 3H), 3.17 (s, 3H), 6.90 (d, J = 8.1 Hz, 1H), 7.24 (d, J = 8.0 Hz, 2H), 7.48 (d, J = 8.1 Hz, 3H), 8.10 (d, J = 8.9 Hz, 1H), 10.58 (s, 1H)

^{13}C NMR (DMSO d_6), δ ppm: 20.7, 43.0, 55.4, 110.2, 122.5, 126.1 (2C), 127.3, 128.1, 129.7 (2C), 134.1, 136.2, 137.2, 141.5, 176.0.

IR ν_{max} (nujol): 3237, 1769, 1738, 1728, 1716, 1620, 1465, 1456, 1201, 836, 741 cm^{-1} .

HRMS (ESI) m/z : $C_{14}H_{12}ClN_2O$ $[M+H]^+$, 316.3748; **Found** 316.3745.



3-Amino-5-(thiophene-2-yl)indole-2-one hydrochloride (42, BB 0300737) was synthesized according to the **GP3** from **42b** (244 mg, 1.00 mmol). Yield: 89%, M = 238 mg. White solid m.p. = 243–245 °C

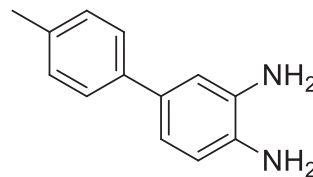
1H NMR (DMSO d_6), δ ppm: 5.02 (s, 1H), 6.96 (d, J = 8.2 Hz, 1H), 7.13 (dd, J = 5.1, 3.6 Hz, 1H), 7.35 (d, J = 3.5 Hz, 1H), 7.50 (d, J = 5.1 Hz, 1H), 7.64 (dd, J = 8.1, 1.3 Hz, 1H), 8.01 (s, 1H), 9.11 (br. s., 3H), 11.02 (s, 1H).

^{13}C NMR (DMSO d_6), δ ppm: 50.7, 110.6, 122.6, 123.2, 124.2, 125.0, 127.3, 127.8, 128.0, 128.0, 128.5, 129.5, 142.4, 143.2, 172.9.

IR ν_{max} (nujol): 2817, 1788, 1702, 1665, 1518, 1432, 1311, 1272, 880 cm^{-1} .

HRMS (ESI) m/z : $C_{12}H_{15}N_2OS$ $[M+H]^+$, 231.0587; **Found** 231.0587.

4'-Methyl-[1,1'-biphenyl]-3,4-diamine (44)

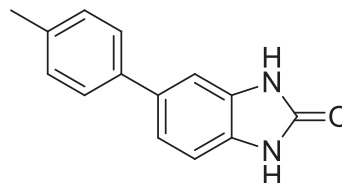


4-Tolylboronic acid (1.35 g, 10 mmol, 1 equiv), was dissolved in mixture of solvents ethanol : water (1:1, 50 mL), then 2-amino-4-bromoaniline **43** (1.87 g, 15 mmol, 1.5 equiv) was added. After 5 min, potassium carbonate (4.14 g, 30 mmol, 3 equiv), triphenylphosphine (105 mg, 4 mmol) and Pd(dba)₂ (115 mg, 2 mmol) were slowly added. The reaction mixture was heated to reflux for 6 h, then cooled to r.t and filtered off. The crude material was washed with diethyl ether and dried under high vacuum. Spectral data are well consistent with the published ones (Seunghee et al., 2013)

Yield: 53%, M = 1.05 g. Brown solid, m.p = 142 °C.

1H NMR (DMSO d_6), δ ppm: 6.62 (d, 2H), 7.16 (t, J = 8.9 Hz, 2H), 7.30 (d, J = 8.4 Hz, 2H), 7.53 (dd, J = 8.7, 5.5 Hz, 2H).

5-(4-Tolyl)-1H-benzimidazole-2(3H)-one (45, BB 0300745)



Compound **44** (396 mg, 2.00 mmol, 1 equiv), was dissolved in DCM (20 mL, 0.1 M). After clear solution forming, CDI was added portion wise (324 mg, 2.00 mmol, 1 equiv) and reaction was stirred for 1 h. The resulting mixture was washed with HCl (0.5 mL, 6.00 mmol, 3 equiv) and the organic layer was dried over sodium sulfate, filtered and evaporated under reduced pressure. Yield: 78%, M = 430 mg. Light-brown solid, m.p = 132–133 °C.

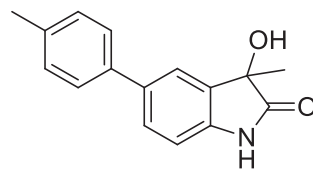
1H NMR (DMSO d_6), δ ppm: 2.32 (s, 3H), 6.98 (d, J = 7.95 Hz, 1H), 7.12 (s, 1H), 7.16–7.29 (m, 3H), 7.47 (d, J = 7.95 Hz, 2H), 10.65 (d, 2H).

^{13}C NMR (DMSO d_6), δ ppm: 20.6, 106.5, 108.8, 119.1, 126.3, 129.1, 129.5, 130.4, 133.0, 135.8, 138.0, 155.5.

IR ν_{max} (nujol): 3257 (br), 2925, 2852, 1732, 1616, 1460, 1377 cm^{-1} .

HRMS (ESI) m/z : $C_{14}H_{13}N_2O$ $[M+H]^+$, 224.2579; **Found** 224.2580.

3-Hydroxy-3-methyl-5-(p-tolyl)indolin-2-one (46, BB 0300751)



5-(p-Tolyl)indoline-2,3-dione (**46a**) (Agamennone et al., 2016) (996 mg, 4.00 mmol, 1 equiv) was dissolved in THF (40 mL, 0.1 M), then under argon atmosphere methylmagnesium bromide (4.36 mL, 0.016 mmol, 4 equiv) was added dropwise at 0 °C. The reaction was warmed to r.t and poured into water solution of HCl (40 mL, 8 e equiv 1 M). The resulting mixture was extracted with ethyl acetate to and dried over sodium sulfate. Organic phase was evaporated under reduced pressure. Yield: 82%, M = 830 mg. White solid, m.p. = 112–114 °C.

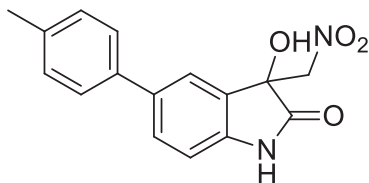
¹H NMR (DMSO *d*₆), δ ppm: 1.41 (s, 3H), 2.32 (s, 3H), 5.93 (br. s., 1H), 6.88 (d, *J* = 7.83 Hz, 1H), 7.24 (d, *J* = 7.46 Hz, 3H), 7.40–7.66 (m, 3H), 10.32 (br. s., 1H).

¹³C NMR (DMSO *d*₆), δ ppm: 20.7, 24.5, 72.8, 110.0, 121.6, 126.0, 127.0, 129.5, 134.0, 134.4, 136.0, 137.4, 140.4, 179.8.

IR vmax (nujol): 3237, 1769, 1738, 1728, 1716, 1620, 1465, 1456, 1201, 836, 741 cm⁻¹.

HRMS (ESI) *m/z*: C₁₆H₁₅NO₂ [M + H]⁺, 254.2958; Found 254.2960.

3-Hydroxy-3-(nitromethyl)-5-(p-tolyl)indolin-2-one (47, BB 0304411)



5-(p-Tolyl)indoline-2,3-dione (**46a**) (Agamennone et al., 2016) (1.00 g, 4.20 mmol, 1 equiv.) was dissolved in nitromethane (12.2 mL, 42.00 mmol, 10 equiv). The reaction was stirred at r.t for 18 h. Then water was added into this mixture and extracted with ethyl acetate. Organic layer was poured into sodium sulfate and evaporated under reduced pressure. Yield: 59%, M = 740 mg. White solid, m.p. = 238 °C.

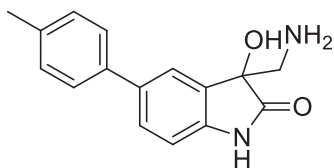
¹H NMR (DMSO *d*₆), δ ppm: 2.33 (br. s., 3H), 4.92–5.20 (m, 2H), 6.77–6.97 (m, 2H), 7.26 (d, *J* = 6.24 Hz, 2H), 7.43–7.60 (m, 3H), 7.73 (br. s., 1H), 10.63 (br. s., 1H).

¹³C NMR (DMSO *d*₆), δ ppm: 20.7, 72.8, 78.2, 110.4, 123.0, 126.0, 128.3, 128.8, 129.6, 134.0, 136.3, 137.0, 141.9, 176.1.

IR vmax (nujol): 2858, 1952, 1754, 1624, 1604, 1541, 1443, 1377, 1306 cm⁻¹.

HRMS (ESI) *m/z*: C₁₆H₁₄N₂O₄ [M + H]⁺, 299.1026; Found 299.1026.

3-(Aminomethyl)-3-hydroxy-5-(p-tolyl)indolin-2-one (48, BB 0304410)



Compound **47** (298 mg, 1.00 mmol, 1 equiv) was dissolved in methanol (10 mL, 0.1 M), then Pd/C 10% (10% mass,) was added. The reaction was stirred under hydrogen atmosphere

over 5 h, then filtered through cellite and filtrate was evaporated under reduced pressure. Yield: 71%, M = 190 mg. White solid, m.p. = 245–247 °C.

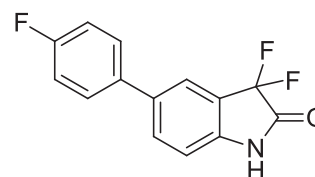
¹H NMR (DMSO *d*₆), δ ppm: 2.33 (s, 3H), 2.76–2.84 (m, 1H), 2.87–2.95 (m, 1H), 6.87 (d, *J* = 8.07 Hz, 1H), 7.24 (d, *J* = 7.95 Hz, 2H), 7.44–7.54 (m, 3H), 7.57 (s, 1H), 10.29 (br. s., 1H).

¹³C NMR (DMSO *d*₆), δ ppm: 20.7, 48.5, 76.2, 109.9, 122.4, 126.1, 127.1, 129.5, 132.0, 133.8, 136.0, 137.5, 141.4, 179.3.

IR vmax (nujol): 3421(br), 3163(br), 2929, 2918, 2854, 1751, 1624, 1462, 1377, 1261 cm⁻¹.

HRMS (ESI) *m/z*: C₁₆H₁₄N₂O₂ [M + H]⁺, 269.1285; Found 269.1281.

3,3-Difluoro-5-(4-fluorophenyl)indolin-2-one (49, BB 0305125)



5-(p-Tolyl)indoline-2,3-dione (**46a**) (Agamennone et al., 2016) (482 mg, 2.00 mmol, 1 equiv) was dissolved in DCM (40 mL, 1 M). Then DAST (1.82 mL, 5.00 mmol, 2.5 equiv) was slowly added by dropwise at –25 °C. Then after 25 min reaction mixture was warmed to r.t and poured into ice. Mixture was extracted and organic layer was dried over sodium sulfate, filtered and evaporated under reduced pressure. Then crude material was triturated with DCM and dried under high vacuum. Yied: 81%, M = 420 mg. White solid, m.p. = 224–225 °C.

¹H NMR (DMSO *d*₆), δ ppm: 7.07 (d, *J* = 8.19 Hz, 1H), 7.28 (t, *J* = 8.80 Hz, 2H), 7.72 (dd, *J* = 8.56, 5.38 Hz, 2H), 7.81 (d, *J* = 8.07 Hz, 1H), 7.97 (s, 1H), 11.30 (br. s., 1H).

¹³C NMR (DMSO *d*₆), δ ppm: 108.8, 112.3, 112.5 (d, *J* = 249.0 Hz), 115.7, 115.9, 116.1 (d, *J* = 21.7 Hz), 120 (t, *J* = 23.3 Hz), 123.2, 128.5 (d, *J* = 8.0 Hz), 132.4, 134.6, 135.3 (d, *J* = 3.2 Hz), 141.8 (t, *J* = 8.0 Hz), 160.7, 163.1, 165.9 (t, *J* = 29.7 Hz).

IR vmax (nujol): 3253(br), 2947, 2922, 2854, 1745, 1716, 1620, 1462, 1377, 1286, 1207, 652 cm⁻¹.

HRMS (ESI) *m/z*: C₁₄H₈F₃NO [M + H]⁺, 264.0631; Found 264.0632.

4.3. MMP inhibition assays

Catalytic domains of MMP-2, –8 and –13 were purchased from Enzo Life Sciences. The assays were performed in triplicate in 96-well black microtiter plates (Corning, NBS). For assay measurements, inhibitor stock solutions (DMSO, 10 mM) were diluted to six different concentrations (1 nM–100 μM) in fluorometric assay buffer (50 mM Tris-HCl pH 7.5, 150 mM NaCl, 1 mM CaCl₂, 1 μM ZnCl₂, 0.05% Brij-35, and 1% DMSO). Enzyme and inhibitor solutions were incubated in the assay buffer for 15 min at room temperature before the addition of the fluorogenic substrate solution (OmniMMP® = Mca-Pro-Leu-Gly-Leu-Dpa-Ala-Arg-NH₂, Enzo Life Sciences, 2.5 μM final concentration or

OmnimMP®RED = TQ3-GABA-Pro-Cha-Abu-Smc-His-Ala-Dab (6'- TAMRA)-Ala-Lys-NH₂, Enzo Life Sciences, 1 μ M final concentration).

After further incubation for 2–4 h at 37 °C, fluorescence was measured ($\lambda_{\text{ex}} = 340$ nm, $\lambda_{\text{em}} = 405$ nm or $\lambda_{\text{ex}} = 545$ nm, $\lambda_{\text{em}} = 572$ nm) using a Perkin-Elmer Victor V3 plate reader. The MMP inhibition activity was expressed as percent inhibition and was calculated from control wells without inhibitor. IC₅₀ values were determined using GraphPad Prism version 5.0 software, and are expressed as mean \pm SEM of at least three independent measurements in triplicate.

4.4. Molecular modeling

The Schrödinger Suite 2019–4 (Schrödinger, 2019) was used for all calculations. Structures of all studied ligands were built in Maestro (Schrödinger, 2019) and submitted to the cxcalc calculation (Chemaxon, 2019) that generates the protonation state at pH 7.4 and possible tautomers. Obtained structures were minimized using MacroModel (Schrödinger, 2019) (force field OPLS-3, minimization algorithm PRCG, convergence on gradient 0.001 kJ/molÅ, the generalized Born/surface area (GB/SA) water solvation model).

3D coordinates of the catalytic domain of MMP-2, MMP-8 and MMP-13 were retrieved from the PDB (PDB IDs: 1QIB, 3DPF and 2OZR respectively). These X-ray structures, selected through a previously reported crossdocking study (Ammazzalorso et al., 2016), were submitted to the Protein Preparation protocol to fix bond orders, H atoms, protonation state, etc. Fixed protein structures were used to produce the grid file used in docking calculations performed by Glide (Schrödinger, 2019).

For the virtual screening campaign, the protocol already described has been applied (Di Pizio et al., 2013), submitting to docking in the MMP-2, –8 and –13 binding site the isatin-based virtual library, in order to prioritize most promising candidates for synthesis.

Synthesized and tested ligands, along with those previously published (Agamennone et al., 2016), were submitted to docking in the previously prepared receptor structures applying both SP and XP protocol. For the study of the binding in the MMP-2 other docking protocols were applied, such as the Induced fit protocol with default settings, and accounting for the possible presence of water molecules. 3D coordinates of water molecules were obtained from both X-ray data (in particular from the structure with PDB ID 3AYU) and from molecular dynamics calculations previously carried out (Ammazzalorso et al., 2016). Several combination of water molecules closer to the binding site have been tried, but just the best performing has been reported, i.e. the one including three water molecules whose position was optimized with a 5-aryl-3-amino-2-oxindole-based ligand.

The ability of the model to discriminate between active and inactive toward MMP-2 has been verified calculating the enrichment values (ROC, AUC, RIE, Table S1).

MD simulation of the MMP-2:37 and MMP-8:37 complexes have been carried out with DesmondS (Schrödinger, 2019). Each complex has been surrounded from an orthorhombic box of SPC water molecules. A preliminary minimization of 2000 iterations to a convergence of 1 kcal/molÅ using the SD and LBFGS algorithms was carried out for each complex.

The production phase of the simulation was forerun by six relaxation steps as by default, and lasted 20 ns, recording frames each 100 ps using a normal pressure temperature (NPT) ensemble with a Nosé-Hoover thermostat at 300 K and Martyna-Tobias-Klein barostat at 1.01325 bar pressure. Smooth Particle Mesh Ewald method was also applied to analyze the electrostatic interactions with a cut-off distance set to 9.0 Å.

Author contributions

Conceptualization and planning, M.A., A.A., A.V.K.; Synthesis and characterization, V.N.I., I.R.I., A.M.N., E.V.M.; biological work, A.L., P.T.; Supervision, A.V.K.; writing original draft, A.V.K., A.A., M.A., A.A.S., writing review and editing, A.V.K., A.A., M.A., A.A.S.

Acknowledgement

The study was funded by the Russian Foundation of Basic Research, project number 20-33-90131.

Declaration of Competing Interest

The authors declare that they have no known competing financial interests or personal relationships that could have appeared to influence the work reported in this paper.

Appendix A. Supplementary material

Supplementary data to this article can be found online at <https://doi.org/10.1016/j.arabjc.2021.103492>.

References

- Adhikari, Nilanjan, Mukherjee, Avinaba, Saha, Achintya, Jha, Tarun, 2017. Arylsulfonamides and selectivity of matrix metalloproteinase-2: an overview. *Eur. J. Med. Chem.* 129, 72–109. <https://doi.org/10.1016/j.ejmech.2017.02.014>.
- Agamennone, M., Belov, D.S., Laghezza, A., Ivanov, V.N., Novoselov, A.M., Andreev, I.A., Ratmanova, N.K., Altieri, A., Tortorella, P., Kurkin, A.V., 2016. Fragment based discovery of 5-arylisatin based inhibitors of matrix metalloproteinases 2 and 13. *Chem-MedChem* 11, 1892–1898. <https://doi.org/10.1002/cmdc.201600266>.
- Amin, Sk Abdul, Adhikari, Nilanjan, Jha, Tarun, 2017. Is dual inhibition of metalloenzymes HDAC-8 and MMP-2 a potential pharmacological target to combat hematological malignancies? *Pharmacol. Res.* 122, 8–19. <https://doi.org/10.1016/j.phrs.2017.05.002>.
- Ammazzalorso, Alessandra, De Filippis, Barbara, Campestre, Cristina, Laghezza, Antonio, Marrone, Alessandro, Amoroso, Rosa, Tortorella, Paolo, Agamennone, Mariangela, 2016. Seeking for non-zinc-binding MMP-2 inhibitors: synthesis, biological evaluation and molecular modelling studies. *Int. J. Mol. Sci.* 17, 1768–1787. <https://doi.org/10.3390/ijms17101768>.
- Babu, K.N., Kinthada, L.K., Das, P.P., Bisai, A., 2018. Cu(II)-tBu-PHOX catalyzed enantioselective malonate addition onto 3-hydroxy 2-oxindoles: application in the synthesis of dimeric pyrroloindoline alkaloids. *Chem. Commun* 54 (57), 7963–7966. <https://doi.org/10.1039/c8cc04338h>.

- Baell, J.B., Holloway, G.A., 2010. New substructure filters for removal of pan assay interference compounds (PAINS) from screening libraries and for their exclusion in bioassays. *J. Med. Chem.* 53, 2719–2740. <https://doi.org/10.1021/jm901137j>.
- Bass, R.J., 2017. Iodination of Isatins. *Tetrahedron Lett.* 16, 1087–1088. [https://doi.org/10.1016/S0040-4039\(01\)96633-X](https://doi.org/10.1016/S0040-4039(01)96633-X).
- Cathcart, J., Pulkoski-Gross, A., Cao, J., 2015. Targeting matrix metalloproteinases in cancer: bringing new life to old ideas. *Genes Dis* 2, 26–34. <https://doi.org/10.1016/j.gendis.2014.12.002>.
- Chemaxon, 2020. <http://www.chemaxon.com>.
- Conlon, Guy A., Murray, Graeme I., 247 (2019),. Recent advances in understanding the roles of matrix metalloproteinases in tumour invasion and metastasis. *J. Pathol.* 247, 629–640. <https://doi.org/10.1002/path.5225>.
- Cui, Ning, Min, Hu, Khalil, Raouf A., 2017. Biochemical and biological attributes of matrix metalloproteinases. *Prog. Mol. Biol. Transl. Sci.* 147, 1–73. <https://doi.org/10.1016/bs.pmbts.2017.02.005>.
- Di Pizio, A., Laghezza, A., Tortorella, P., Agamennone, M., 2013. Probing the S1' site for the identification of non-zinc-binding MMP-2 inhibitors. *ChemMedChem* 8, 1475–1482. <https://doi.org/10.1002/cmdc.201300186>.
- Di Pizio, A., Agamennone, M., Tortorella, P., 2016. Non-zinc-binding inhibitors of MMP-13: GRID-based approaches to rationalize the binding process. *Curr. Top. Med. Chem.* 16, 449–459. <https://doi.org/10.2174/1568026615666150813150631>.
- Dublanchet, A.-C., Ducrot, P., Andrianjara, C., O'Gara, M., Morales, R., Compère, D., Denis, A., Blais, S., Cluzeau, P., Courté, K., Hamon, J., Moreau, F., Prunet, M.-L., Tertre, A., 2005. Structure-based design and synthesis of novel non-zinc chelating MMP-12 inhibitors. *Bioorg. Med. Chem. Lett.* 15, 3787–3790. <https://doi.org/10.1016/j.bmcl.2005.05.079>.
- Dufour, A., Overall, Christopher M., 2013. Missing the target: matrix metalloproteinase antitargets in inflammation and cancer. *Trends Pharmacol. Sci.* 34, 233–242. <https://doi.org/10.1016/j.tips.2013.02.004>.
- Engel, Christian K., Pirard, Bernard, Schimanski, Sandra, Kirsch, Reinhard, Habermann, Jörg, Klingler, Otmar, Schlotte, Volkhard, Weithmann, Klaus Ulrich, Ulrich Wendt, K., 2005. Structural basis for the highly selective inhibition of MMP-13. *Chem. Biol.* 12, 181–189. <https://doi.org/10.1016/j.chembiol.2004.11.014>.
- Fabre, B., Ramos, A., de Pascual-Teresa, B., 2014. Targeting matrix metalloproteinases: exploring the dynamics of the s1' pocket in the design of selective, small molecule inhibitors. *J. Med. Chem.* 57, 10205–10219. <https://doi.org/10.1021/jm500505f>.
- Fields, Gregg B., 2019. The rebirth of matrix metalloproteinase inhibitors: moving beyond the dogma. *Cells* 8, 984–1008. <https://doi.org/10.3390/cells8090984>.
- Fischer, T., Senn, N., Riedl, R., 2019. Design and structural evolution of matrix metalloproteinase inhibitors. *Chem. Eur. J.* 25, 7960–7980. <https://doi.org/10.1002/chem.201805361>.
- Gérard, A.-L., Lisowski, V., Rault, S., 2005. Direct synthesis of new arylanthranilic acids via a Suzuki cross-coupling reaction from iodoisatins. *Tetrahedron* 61, 6082–6087. <https://doi.org/10.1016/j.tet.2005.04.022>.
- Gimeno, A., Beltrán-Debón, R., Mulero, M., Pujadas, G., Garcia-Vallvé, S., 2020. Understanding the variability of the S1' pocket to improve matrix metalloproteinase inhibitor selectivity profiles. *Drug Discov. Today* 25, 38–57. <https://doi.org/10.1016/j.drudis.2019.07.013>.
- Holmquist, M., Blay, G., Pedro, J.R., 2014. Highly enantioselective aza-Henry reaction with isatin N-Boc ketimines. *Chem. Commun.* 50, 9309–9312. <https://doi.org/10.1039/c4cc04051a>.
- Huifeng, Yue, Lin, Guo, Hsuan-Hung, Liao, Cai, Yunfei, Chen, Zhu, Magnus, Rueping, 2017. Catalytic ester and amide to amine interconversion: nickel-catalyzed decarbonylative amination of esters and amides by C–O and C–C bond activation. *Angew. Chem. Int. Ed.* 56 (15), 4282–4285.
- Justo, Lorenzo Antonio, Durán, Rafael, Alfonso, Miguel, Fajardo, Daniel, Faro, Lilian Rosana F., 2016. Effects and mechanism of action of isatin, a MAO inhibitor, on in vivo striatal dopamine release. *Neurochem. Int.* 99, 147–157. <https://doi.org/10.1016/j.neuint.2016.06.012>.
- Juurikka, K., Butler, G.S., Salo, T., Nyberg, P., Åström, P., 2019. The role of MMP8 in Cancer: a systematic review. *Int. J. Mol. Sci.* 20, 4506–4533. <https://doi.org/10.3390/ijms20184506>.
- King, S.E., 2016. Matrix metalloproteinases: new directions toward inhibition in the fight against cancers. *Future Med. Chem.* 8, 297–309. <https://doi.org/10.4155/fmc.15.184>.
- Kudo, Y., Iizuka, S., Yoshida, M., Tsunematsu, T., Kondo, T., Subarnbhesaj, A., Deraz, Elsayed M., Siriwardena, Samadarani B. S.M., Tahara, Hidetoshi, Ishimaru, Naotomi, Ogawa, Ikuko, Takata, Takashi, 2012. Matrix metalloproteinase-13 (MMP-13) directly and indirectly promotes tumor angiogenesis. *J. Biol. Chem.* 287, 38716–38728. <https://doi.org/10.1074/jbc.M112.373159>.
- Laghezza, A., Luisi, G., Caradonna, A., Di Pizio, A., Piemontese, L., Loiodice, F., Agamennone, M., Tortorella, P., 2020. Virtual screening identification and chemical optimization of substituted 2-arylbenzimidazoles as new non-zinc-binding MMP-2 inhibitors. *Bioorganic Med. Chem.* 28, 115257. <https://doi.org/10.1016/j.bmc.2019.115257>.
- Lisowski, V., Robba, M., Rault, S., 2000. Efficient synthesis of novel 3-(het)arylanthranilic acids via a suzuki cross-coupling reaction of 7-iodoisatin with (het)arylboronic acids in water. *J. Org. Chem.* 65, 4193–4194. <https://doi.org/10.1021/jo991948i>.
- Nakamura, Yu, Yoshida, Suguru, Hosoya, Takamitsu, 2017. Facile synthesis of phthalides from methyl ortho-iodobenzoates and ketones via an iodinemagnesium exchange reaction using a silylmethyl grignard reagent. Facile synthesis of phthalides from methyl ortho-iodobenzoates and ketones via an iodinemagnesium exchange reaction using a silylmethyl grignard reagent. *Chem. Lett.* 46 (6), 858–861.
- Nakao, S., Mabuchi, M., Shimizu, T., Itoh, Y., Takeuchi, Y., Ueda, M., Mizuno, H., Shigi, N., Ohshio, I., Jinguji, K., Ueda, Y., Yamamoto, M., Furukawa, T., Aoki, S., Tsujikawa, K., Tanaka, A., 2014. Design and synthesis of prostate cancer antigen-1 (PCA-1)/ALKBH3 inhibitors as anti-prostate cancer drugs. *Bioorg. Med. Chem. Lett.* 24, 1071–1074. <https://doi.org/10.1016/j.bmcl.2014.01.008>.
- Natsumi, I., Takeshi, F., Tatsuya, M., Sakura, Y., Mamoru, H., Morio, N., 2018. Synthesis and characterization of radioiodinated 3-phenethyl-2-indolinone derivatives for SPECT imaging of survivin in tumors. *Bioorg. Med. Chem.* 26 (12), 3111–3116. <https://doi.org/10.1016/j.bmc.2018.04.034>.
- Overall, Christopher M., Kleifeld, Oded, 2006. Tumour microenvironment – opinion: validating matrix metalloproteinases as drug targets and anti-targets for cancer therapy. *Nat. Rev. Cancer* 6, 227–239. <https://doi.org/10.1038/nrc1821>.
- Pakravan, P., Kashanian, S., Khodaei, M.M., Harding, F.J., 2013. Biochemical and pharmacological characterization of isatin and its derivatives: from structure to activity. *Pharmacol. Rep.* 65, 313–335. [https://doi.org/10.1016/s1734-1140\(13\)71007-7](https://doi.org/10.1016/s1734-1140(13)71007-7).
- Pochetti, G., Montanari, R., Gege, C., Chevrier, C., Taveras, A.G., Mazza, F., 2009. Extra binding region induced by non-zinc chelating inhibitors into the S1' subsite of matrix metalloproteinase 8 (MMP-8). *J. Med. Chem.* 52 (2009), 1040–1049. <https://doi.org/10.1021/jm801166j>.
- Poupaert, J., Carato, P., Colacino, E., 2005. 2(3H)-benzoxazolone and bioisosters as “Privileged Scaffold” in the design of pharmacological probes. *Curr. Med. Chem.* 12, 877–885. <https://doi.org/10.2174/0929867053507388>.
- Schmidt, B., Elizarov, N., Riemer, N., Hölter, F., Salts, A., 2015. Opportunities for multiple arenefunctionalization. *Eur. J. Org. Chem.* 2015 (26), 5826–5841. <https://doi.org/10.1002/ejoc.201500795>.

- Schrödinger Release, 2019. 2019-4: Maestro, Glide, LigPrep, Macro-Model, Desmond Molecular Dynamics System, New York, NY.
- Seunghye, H., Jinhee, K., Sun-Mi, Y., Hyunseung, L., Yoonsu, P., Soon-Sun, H., Hong, Sungwoo, 2013. Discovery of new benzothiazole-based inhibitors of breakpoint cluster region-abelson kinase including the T315I mutant. *J. Med. Chem.* 56 (9), 3531–3545. <https://doi.org/10.1021/jm301891t>.
- Shay, G., Tauro, M., Loiodice, F., Tortorella, P., Sullivan, D.M., Hazlehurst, L.A., Lynch, C.C., 2017. Selective inhibition of matrix metalloproteinase-2 in the multiple myeloma-bone microenvironment. *Oncotarget* 8, 41827–41840 <https://doi.org/10.18632/oncotarget.18103>.
- Sternlicht, Mark D., Werb, Zena, 2001. How Matrix metalloproteinases regulate cell behavior. *Annu Rev. Cell Dev. Biol.* 17, 463–516. <https://doi.org/10.1146/annurev.cellbio.17.1.463>.
- Tauro, M., Lynch, C.C., 2018. Cutting to the chase: how matrix metalloproteinase-2 activity controls breast-cancer-to-bone metastasis. *Cancers* 10, 185–199. <https://doi.org/10.3390/cancers10060185>.
- Thirkettle, S., Decock, J., Arnold, H., Pennington, Caroline J., Jaworski, Diane M., Edwards, Dylan R., 2013. Matrix metalloproteinase 8 (collagenase 2) induces the expression of interleukins 6 and 8 in breast cancer cells. *J. Biol. Chem.* 288, 16282–16294. <https://doi.org/10.1074/jbc.M113.464230>.
- Vandenbroucke, R.E., Libert, C., 2014. Is there new hope for therapeutic matrix metalloproteinase inhibition? *Nat. Rev. Drug Discov.* 13, 904–927. <https://doi.org/10.1038/nrd4390>.
- Wang, C.H., White, A.R., Schwartz, S.N., Alluri, S., Cattabiani, T.M., Zhang, L.K., Chan, T.M., Buevich, A.V., Ganguly, A.K., 2012. Novel synthesis and functionalization of ortho–ortho disubstituted biphenyls and a highly condensed novel heterocycle using radical cyclization reaction. *Tetrahedron* 68 (47), 9750–9762. <https://doi.org/10.1016/j.tet.2012.09.036>.
- Winer, A., Janosky, M., Harrison, B., Zhong, J., Moussai, D., Siyah, P., Schatz-Siemers, N., Zeng, J., Adams, S., Mignatti, P., 2016. Inhibition of breast cancer metastasis by presurgical treatment with an oral matrix metalloproteinase inhibitor: a preclinical proof-of-principle study. *Mol. Cancer Ther.* 15, 2370–2377. <https://doi.org/10.1158/1535-7163.MCT-16-0194>.
- Winer, A., Adams, S., Mignatti, P., 2018. Matrix metalloproteinase inhibitors in cancer therapy: turning past failures into future successes. *Mol. Cancer Ther.* 17, 1147–1155. <https://doi.org/10.1158/1535-7163.MCT-17-0646>.
- Witschel Matthias, C., Matthias, Rottmann, Anatol, Schwab, Uboisree, Leartsakulpanich, Penchit, Chitnumsub, Michael, Seet, Sandro, Tonazzi, Pimchai, Chaiyen, François, Diederich, 2015. Inhibitors of plasmoidal serine hydroxymethyltransferase (SHMT): cocrystal structures of pyrazolopyrans with potent blood- and liver-stage activities. *J. Med. Chem.* 58 (7), 3117–3131.
- Young, D., Das, N., Anowai, A., Dufour, A., 2019. Matrix Metalloproteases as Influencers of the Cells' Social Media. *Int. J. Mol. Sci.* 20, 3847–3867. <https://doi.org/10.3390/ijms20163847>.
- Zhang, Q., Teng, Y., Yuan, Y., Ruan, T., Wang, Q.i., Gao, X., Zhou, Y., Han, K., Peng, Y.u., Kui, L.u., 2018. Synthesis and cytotoxic studies of novel 5-phenylisatin derivatives and their anti-migration and anti-angiogenic evaluation. *Eur. J. Med. Chem.* 156, 800–814. <https://doi.org/10.1016/j.ejmech.2018.07.032>.
- Zhong, Y., Yu-Ting, L.u., Sun, Y., Shi, Z.-H., Li, N.-G., Tang, Y.-P., Duan, J.-A., 2018. Recent opportunities in matrix metalloproteinase inhibitor drug design for cancer. *Expert Opin. Drug Discov.* 13, 75–87. <https://doi.org/10.1080/17460441.2018.1398732>.